Urea for CO_2 Capture: A Theoretical Investigation

submitted by

Piers Townsend

for the degree of Master of Research

of the

University of Bath

Center for Sustainable Chemical Technologies

September 2019

Signed on behalf of the Faculty of Science .....

Abstract

Climate change and global warming are two of the biggest issues facing modern science. The atmospheric carbon dioxide concentration has increased rapidly since the industrial revolution, and finding novel technologies to support carbon capture, storage and utilisation (CCSU) is vital in reducing the risk of catastrophic climate change. Urea is a low-cost, bio-based material that is produced in large quantities every year. It has been hypothesised that urea shows the pre-requisite chemical functionality to perform as an adsorbent for carbon capture. This study examines the adsorption of CO_2 on the most common surfaces observed in phase I, phase III and phase IV of urea. Density functional theory was used to relax the crystalline geometries, and results showed that ambient phase urea is the most stable crystal morphology. Furthermore, grand canonical Monte Carlo was used to simulate both single component CO_2 and mixed component CO_2/N_2 adsorption isotherms. Results indicate that the (001) surface of phase I urea has the highest overall selectivity and adsorption capacity towards CO_2. At 298 K and 1 bar, the (001), (100) and (010) surfaces showed excess adsorption capacities of 0.250, 0.061, and 0.184 mmol/g respectively. The results showed that crystalline urea shows relatively poor performance when compared to other physical adsorbents such as activated carbons and zeolites.

Acknowledgements

First and foremost, I would like to acknowledge Dr. Matthew Lennox for his on-going support over the last couple of months. Our meetings have been extremely beneficial, and I have learned many new things from his support and expertise. I would also like acknowledge Prof. Tina Duren for being incredibly kind, patient and supportive throughout the course of this project - Prof. Duren did not form part of my supervisory team and I am therefore very grateful for the time that was given.

Furthermore, I would like to acknowledge Dr. Joe Manning for his incredible support and infinite patience. Without his support, learning to use MuSIC would have been substantially more difficult and I cannot emphasise enough the role he had to play in my learning. Thank you Joe.

Lastly, I would like to acknowledge Megan Thompson for her support and patience in learning to use CrystalMaker. She taught me how to wonderfully cut a crystal, and was the first person to successfully help me visualise crystal faces. Again, I cannot emphasise enough my appreciation for her support.

Thank you to all involved.

List of Figures

List of Tables

Abbreviations

Abbreviations	Definition
UNFCCC	United Nations Framework Convention on Climate Change
GHG	Greenhouse Gas
IUPAC	International Union of Pure and Applied Chemistry
IPCC	International Panel on Climate Change
JPI	Japan Petroleum Institute
CCSU	Carbon Capture, Storage and Utilisation
CO_2	Carbon Dioxide
N_2	Nitrogen
CCDC	Cambridge Crystallographic Data Centre
AC	Activated Carbon
MD	Molecular Dynamics
GCMC	Grand Canonical Monte Carlo
MC	Monte Carlo
DFT	Density Functional Theory
KS	Kohn-Sham
MOF	Molecular Organic Framework
CG	Conjugate Gradient

Contents

Chapter 1

Introduction

1.1 Climate Change

'Climate change' is a phrase that most people will have heard on television, read in a newspaper, or studied in school. However, for many in the scientific community, climate change remains the most fundamental problem facing mankind in the twenty-first century.[1] Defining climate change may appear simple at first glance, but many formal definitions exist. One such example is from the United Nations Framework Convention on Climate Change, where they define it as "a change of climate which is attributed directly or indirectly to human activity that alters the composition of the global atmosphere and which is in addition to natural climate variability observed over comparable time periods". More generally though, it can be defined as a long-term change in the distribution of weather patterns over a given period of time.[2]

1.1.1 A Brief History on Climate Change

Around 30 years ago, one of the worlds most prominent climate scientists James Hansen testified to a U.S. Congress committee. He argued that both he and his associates at the National Aeronautics and Space Administration were unequivocally sure that the gradual trends in global warming, related to atmospheric gases such as carbon dioxide and methane; so-called 'greenhouse

gases'.[3] Following this in 1990, further warnings of the disastrous consequences of global climate change continued to infilitrate scientific literature.[4,5] As we moved towards the beginning of the new millennium, science was appearing to be less receptive towards the idea of catastrophic, civilization-destroying climate change. As the years have progressed, however, and we look forward to modern times, climate change acceptance has become more widespread.[6] Arguably, one of the most important changes within climate change policy was the introduction of the Paris agreement as put forward by the UNFCCC. The overarching aims of this policy were to initiate and encourage a global response to the threat of global warming, whilst simultaneously ensuring that the mean global temperature doesn't rise more than 2 degrees Celsius above values associated with the pre-industrial era.[7] As of early 2019, 194 states have signed and accepted the Paris agreement, with over 85% of global emissions being accounted for by the combination of these countries. It is worth noting that controversy and disagreement will always exist when it comes to the acceptance of global warming. Despite this, it is readily agreed within the scientific community that moving towards a low-carbon future is imperative in ensuring sustainable development, and reducing the risk of catastrophic climate change.

1.1.2 Greenhouse Gas Emissions

The challenge of deeply reducing the emission of greenhouse gases (GHG) is one which faces the modern world. This is no easy task, due to societies reliance on the burning of fossil fuels for low-cost energy production across the globe. Many anthropogenic industrial activities contribute towards GHG emission: electricity production, transportation, agriculture, and materials manufacture (e.g. steel and iron processing) to name but a few.[8] In the pre-industrial era (around 1750), the atmospheric carbon dioxide concentration was approximately 280 ppm and had remained that way for thousands of years. Since then, it has continued to increase to around 370 ppm in 2000, and has now reached a high of 413 ppm in 2019.[9] Furthermore, it has been ascertained that atmospheric carbon dioxide concentrations are increasing at approximately 2 ppm per annum, which is unsustainable when it comes to a long-term outlook on climate. To illustrate these rapidly occurring changes, Figure 1 shows the increase in the atmospheric

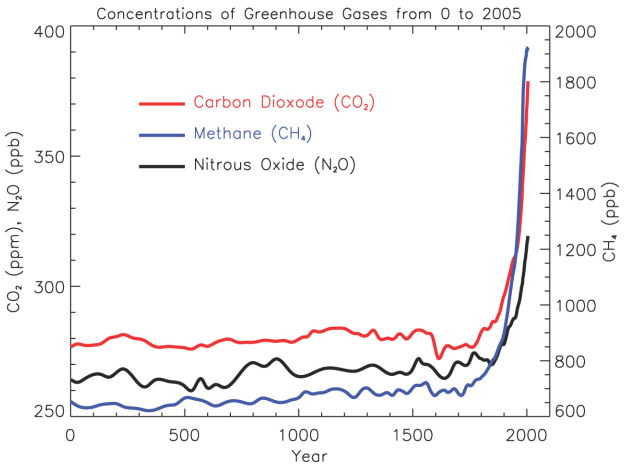

Figure 1: Changes in atmospheric carbon dioxide, methane and nitrous oxide concentrations over the the last 2000 years.

concentrations of carbon dioxide, methane, and nitrous oxide over the last two thousand years. There are many different types of GHG, however, climate change is an issue primarily caused by increasingly high levels of carbon dioxide in the atmosphere. Radiative forcing (RF) is a key parameter in climate science, and as a metric, can be linked to different atmospheric constituents. Climate drivers, such as carbon dioxide, are known to have high radiative forcing values; this means that a net increase in heat will reach the earths surface due to that **specific** climate driver. In 2007, the IPCC showed that carbon dioxide has the highest RF value when compared to other greenhouse gases such as methane and halocarbons, thus indicating the huge role that carbon dioxide has to play in global warming.[10] Furthermore, in a 2018 report, the IPCC predict with high confidence that if we can reach and sustain global net zero carbon dioxide emissions, natural atmospheric radiative forcing will prevent further human-induced global warming over a period of decades. The IPCC also set a target of reducing global carbon dioxide emissions by 40 - 72% by 2050. This brief introduction hopes to illustrate the severity of the situation we face, and demonstrates the urgent need to develop new, innovative solutions to capturing, storing and utilising atmospheric carbon dioxide.

Chapter 2

Background Information

2.1 Carbon Capture, Storage and Utilisation

Mitigating the risk of climate change requires a multi-level approach. There exists a number of ways in which whole nations, large (or small) companies and individual people can reduce their carbon footprint, such as:

- Utilisation of renewable energy sources where possible; e.g. wind, solar and hydroelectric.
- Increase the usage of fuels with low carbon emissions e.g. hydrogen, natural gas.
- Apply geoengineering methodologies such as the reforestation of land.
- **CO_2 capture and storage.**

Each of these approaches has advantages and disadvantages. However, to reduce CO_2 emissions on a global scale, and meet the IPCC requirements of a 40 - 72% reduction, it is likely that a **mixture** of these methodologies will be part of the solution.

As a field, carbon capture, storage and utilisation (CCSU) has a vast array of technologies embedded within it. The direct capture of carbon is itself only part of the process, with transportation, separation, monitoring, and storage being key processes to consider. Futhermore, in recent years, there has been a shift away from simply capturing and storing carbon; the circular economy supports

the idea of utilising captured carbon as a valuable material.[11] Prior to this, the focus of CCS was to transport CO_2 and store it within geological formations such as depleted oil/gas fields or saline aquifers. Compared to the methods discussed at the beginning of this section, carbon capture and storage offers the potential to remove large amounts of CO_2 from point emission sources such as industrial factories and power generation facilities.[12] Therefore, permitting a sufficient purity of CO_2 can be obtained from the chosen capture technology, utilisation in place of storage is a highly viable endpoint. Before moving forward, let us first consider the three available routes for capturing carbon dioxide:

Post-Combustion Carbon Capture This method involves the capture of CO_2 from a flue gas, post-combustion. The concentration of CO_2 in a flue gas is typically quite low (between 4 - 14 %), and this leads to high capital costs associated with the separation process. These high costs are due to the purity requirements for the transport and storage of captured CO_2 (> 95 %).[13] In 2015, there were 16 large-scale carbon capture facilities in commercial operation. However, only two of these facilities utilised post-combustion carbon capture.[14]

Pre-Combustion Carbon Capture This method involves pre-treating fossil fuel derived commodity chemicals prior to their burning. The typical pre-treatment for coal involves gasification under low O_2 concentrations, leading to formation of a syngas that consists of primarily H_2 and CO. A water-gas shift reaction occurs, whereby CO is converted into CO_2 whilst water is converted into hydrogen. The waste CO_2 is then separated and collected whilst the hydrogen is utilised and burnt as a fuel.

Oxyfuel Combustion The primary idea behind this methodology involves the burning of pure oxygen gas instead of air. This reduces the concentration of nitrogen in exhaust gases, thereby making the separation of CO_2 easier. Water and particulates continue to be an issue in terms of flue gas composition, but these can be readily be removed with standard techniques such as desulfurization.

The sections above categorise **where** the gas is captured in terms of the industrial process. Importantly, one common theme underpins all of these methods: the **physical separation** of CO_2 from other gases. For this reason, the separation process remains to be the focus of much scientific attention.

2.2 Methodologies for CO_2 Separation

There exists a plethora of technologies for the separation of CO_2, and the choice of process typically relates to the purity and state of CO_2 prior to separation. Membrane separations, cryogenic distillation, hydrate-based separation, and chemical looping are just a few of the methods available for the separation of CO_2. However, many of these methodologies face challenges due to their high energy demand and costs of production.[15] This work will discuss the two most commercially utilised methods: liquid amine-based absorption and solid physisorptive adsorption.

2.2.1 Absorption Processes

According to IUPAC nomenclature, absorption can be defined as 'The process of one material (absorbate) being retained by another (absorbent)'. The key difference between absorption and adsorption relates to the mode of action; in absorption, molecules are retained and taken up by the volume whilst in adsorption, molecules are only taken up by the surface of the adsorbent.[16] The research and development into novel absorbents for the separation of CO_2 from flue gas has existed for over a century. Among the variety of reactive solvents used for post-combustion carbon capture (e.g. chilled ammonia or ionic liquids), the best known and most commonly used chemical absorbents are aqueous alkanolamines. These have been in use for a long period of time, and a 20 - 30 wt% solution of monoethanolamine is typically considered to be the gold standard. The process was first patented by Bottoms in 1930, and was originally developed for the removal of H_2S and CO_2 from natural gas; so-called 'acid gas sweetening' or 'amine scrubbing'.[17] Since the discovery of amine scrubbing, it has been widely utilised by industry and is best suited for applications that involve low partial pressures of CO_2. For this reason, it has become the benchmark process for electricity generation plants.[18]

Although monoethanolamine has been the most widely used sorbent for many years, it is relatively toxic, and a variety of different amine-based sorbents have been studied for their use in acid gas sweetening. Understanding the energy performance of these solvents is vitally important to ensure that capital

costs don't become too high. The energy performance of a sorbent is typically governed by four properties: liquid absorption capacity for CO_2, the rate of CO_2 absorption, the heat of CO_2 absorption and the temperature of thermal degradation.[19] Piperazine, and piperazine blends have previously shown excellent promise as next generation carbon capture sorbents. A 30 wt% piperazine solution has been shown to have CO_2 absorption rates 2.5 times faster than 7 m MEA, along with a 22 % greater CO_2 absorption capacity.[19,20] A recent study by van de Ham *et al* calculated the net electric power plant efficiency for both an MEA and a piperazine-based process in four different power plant models. They showed that piperazine-based processes have a $\approx$ 2% higher efficiency than MEA-based processes, and if energy performance is the most valued metric, piperazine-based carbon capture processes are superior.[21]

In most cases, amine scrubbing relies on the use of thermal-swing regeneration. A gas stream with high carbon dioxide concentration is first passed into an absorption column at elevated pressures and is scrubbed with a low temperature, 'lean' (low CO_2) amine stream. An exhaust gas with a low CO_2 concentration leaves from the top of the absorption column, whilst the 'rich' amine (high CO_2) stream leaves from the bottom. Then, the rich stream is pumped into a high temperature, low pressure stripping column. These conditions heavily favour the desorption of CO_2, and a gas stream with high CO_2 concentration ($>$ 99.5 %) exits from the top of the stripping column (see Figure 2).[19]

This 'prototypical' process has been favoured by industry for over fifty years and continues to be in operation. Unfortunately though, the construction of amine-based carbon-capture plants has not been widespread due to the number of issues attached to the process. Firstly, the process is extremely energy intensive due to a high parasitic energy consumption during the process of solvent regeneration. Despite fast kinetics, the energy required for solvent regeneration is typically in the range of 3.0 - 4.2 GJ/tonne of CO_2.[22] Whilst gas-powered turbines (that utilise natural-gas and coal) continue to be the primary method for electricity generation, this process will never be sustainable in the long-term. Furthermore, issues exist with both solvent degradation and corrosion. Thermal and oxidative degradation are both factors to consider when designing a process. In the case of amine scrubbing, oxidative degradation

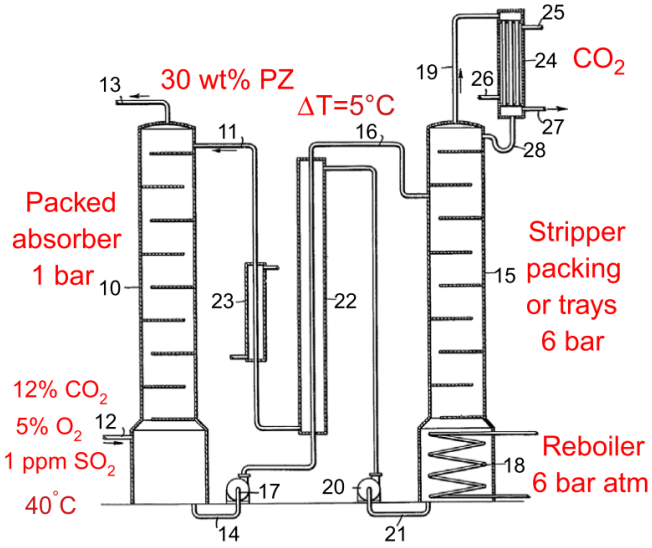

Figure 2: The process for acid-gas sweetening as patented by Bottoms in 1930. The absorption column and stripping column are used in a thermal swing regeneration process.[19]

is typically more problematic than thermal. The mechanism for oxidative degradation is not well understood. However, it has been established that when iron, copper or manganese ions come into contact with the absorbent, amine oxidation will occur.[23] Lastly, corrosion of the amine treating equipment is an issue for two main reasons: an increase in capital costs due to repair and an increase in the risk of environmental contamination. To illustrate the magnitude of the problem, a survey conducted by the JPI reported a 72 % occurrence of stress corrosion-based cracking at amine plants throughout Japan.[24] To summarise, traditional amine scrubbing is a dominant technology that has shown great promise since its inception. Despite its dominance, the process does suffer from issues that need correcting; without a solution to these problems, the process will never be fully viable in the long-term. It is evident that more research is needed to explore new, sustainable, non-toxic materials for post-combustion carbon capture.

2.2.2 Adsorption Processes

This section will examine the use of adsorptive separation techniques in the field of carbon capture, storage and utilisation. As a process, adsorption can be

defined as the 'adhesion of atoms, molecules or ions from a fluid or dissolved solid onto a surface'. There are two primary ways in which atoms and molecules can adsorb onto a surface (see Figure 3).[25] **Chemisorption** involves the formation of specific covalent bonds, typically originating from electrostatic interactions, and also shows high enthalpies of adsorption ($\approx -$ 200 kJ/mol). In **physisorption**, no bonds are formed, interactions are governed by van der Waals forces, and perturbation of the electronic states of the adsorbate and adsorbent are minimal. Futhermore, physisorption shows low enthalpies of adsorption, typically in the region of $-$ 20 kJ/mol.

When compared to traditional amine-based absorption methods, adsorptive technologies have the major advantage of reduced energy demand attached to adsorbent regeneration.[26] The process of absorbent regeneration accounts for most of the power requirement in amine scrubbing, and developing new materials that drastically reduce operating costs is vital in furthering the sustainable development of new, efficient, next-generation carbon capture processes. Meeting certain guidelines is the biggest challenge in the design of new materials for the separation of CO_2 from flue gas. For example, the Department of Energy set quantitative guidelines for newly developed carbon capture technologies, such as: electricity costs attached to the process should not increase by more than 35 %, whilst simultaneously ensuring that 90 % of exiting CO_2 is captured.[27] This is extremely challenging due to the large number of factors to consider when assessing new adsorbents for CO_2 separation: (1) long-term adsorbent stability, (2) adsorbent durability, (3) CO_2 selectivity, (4) adsorption capacity and (5) ease of adsorbent regeneration. It has previously been reported that costs can be reduced if physical adsorption based methods are adopted in place of liquid-solvent absorption methods such as amine scrubbing.[28] In recent years,

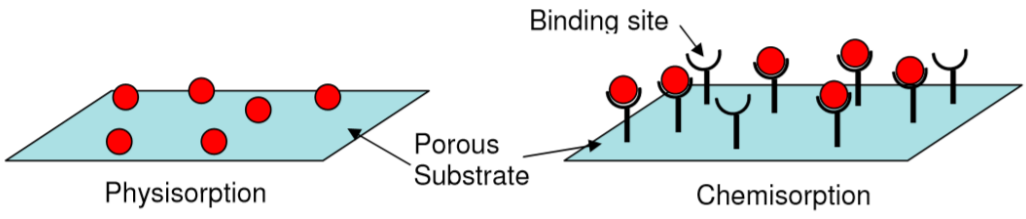

Figure 3: A graphic illustration of physisorption and chemisorption. Phyisorption is non-specific and governed by Van de Waals interactions.[25]

two adsorption technologies have been the focus of much attention for use in industrial scale carbon capture.

Pressure/Vacuum Swing Adsorption (PSA/VSA) This process was first patented in 1932 and is considered relatively inexpensive when compared to other technologies.[29] Regeneration of the adsorbent material is achieved by lowering the internal pressure of the adsorption column; the system is 'swung' between high and low pressures to respectively induce adsorption and desorption. In PSA, the adsorption step is carried out at pressures > 1 atm, whilst in VSA, the pressures used for adsorption are < 1 atm.

Temperature Swing Adsorption (TSA) Temperature swing adsorption involves the use of a low temperature state to induce adsorption, followed by an increase in temperature to induce desorption. To initiate adsorbent regeneration, the adsorption bed temperature is increased using a stream of hot gas. Once regeneration is complete, a stream of cold gas is used to cool the adsorption bed prior to starting another adsorption cycle.[26] TSA has two main problems associated with it: a large energy requirement attached to the desorption step, and the inability to quickly cycle the adsorption bed temperature.

The literature shows that much work has been carried out looking at both PSA and TSA for post-combustion carbon capture.[30–32] PSA is traditionally the favoured method when the concentration of the removed components (in this case, carbon dioxide) is an important factor in the process.[33] Habib *et al* further corroborate this by discussing how PSA is the better option due to ease of application, lower energy costs and lower capital investments.[26] Before designing one of these processes, selection of the adsorbent material type is a fundamental stage in development. For this reason, many materials have been investigated for their suitability in adsorption-based carbon capture.

2.3 Materials for Use in Physisorptive Carbon Capture

Over the years, many different material classes have been identified for use in adsorptive carbon capture. Generally, these materials can be separated into one of two categories: (i) physical adsorbents and (ii) chemical adsorbents. Physical adsorbents are governed by non-covalent Van de Waals interactions, and show greater energy efficiencies when compared to chemical adsorbents. For this reason, there is considerable interest in physical adsorbents for carbon capture. Improved energy efficiencies are attributed to the adsorbent regeneration process; ensuring a delicate balance between affinity for the adsorbate and cost of regeneration is vital in minimising energy costs. With physical adsorbents, structural disturbance of the molecular framework is minimal, and pore size plays an important role in determining the extent of adsorption and adsorbate selectivity. According to IUPAC nomenclature, pore sizes are defined by: < 2 nm for micro-pores, between 2 - 50 nm for meso-pores, and > 50 nm for macro-pores. For carbon capture, micro-pores are best suited for a highly selective separation of CO_2. In this section, a variety of materials will be examined for their potential use in physisorptive carbon capture.

2.3.1 Zeolites

Zeolites are microporous materials, commonly used in both catalytic and adsorption processes. The crystal structure, and therefore the zeolite type, is dependent on the 3-dimensional structure of the primary and secondary building units (SBU's). Zeolites are crystalline tectoaluminosilicates composed of building blocks such as SiO_4 and AlO_4, and have pore sizes ranging from 0.3 nm - 1 nm (see Figure 4). When Si is substituted for Al, a negative charge is introduced into the framework, and the excess charge is then balanced by rare earth metal ions such as Na^+, Mg^+ and Ca^+.[34]

In the literature, many of these materials have been investigated for their use in CO_2 separation. The kinetic diameter of CO_2 is 330 pm, meaning that zeolites can separate CO_2 via a molecular sieving effect.[35] At low temperatures, zeolites show preferential adsorption of CO_2 when compared to other gases such as N_2 and H_2.

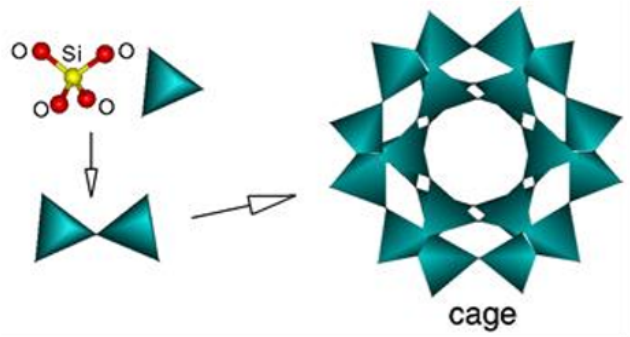

Figure 4: By combining primary building units (PBU's), secondary building units (SBU's) are formed which arrange themselves in space differently for each zeolite type.

This can be explained by the higher quadrupole moment and polarizability of CO_2. Furthermore, it's important to note that adsorption capacities decrease with higher operating temperatures. Tang *et al* used gas chromotography to measure the CO_2 adsorption capacities for three commonly used industrial zeolites: NaX, CaX and NaY.[36] The best performing zeolites were NaX and NaY, showing an adsorption capacity of 5.71 and 5.50 mmol/g respectively at 32°C. Meanwhile, CaX showed an adsorption capacity of 3.40 at 30°C. At first, these capacities appear very good, however, these values are measured at relatively low temperatures. Industrial processes emit flue gas at higher temperatures; upon emission, the temperature of a flue gas is typically 1200°C. Once the flue gas has reached the separation process, however, its temperature typically sits around 60°C. The performance of zeolites for CO_2 adsorption is drastically effected by higher temperatures - before zeolites can be commercially utilised, more research is needed to develop mechanisms that allow adsorption at higher temperatures. The evidence above suggests that zeolites are not currently the best commercial candidates for post-combustion carbon capture.

2.3.2 Metal Organic Frameworks (MOF's)

Around two decades ago, a new class of materials called 'Metal Organic Frameworks' (or MOF's) were discovered. They are a group of crystalline, porous solids with very high internal surface areas; of all materials currently characterized, MOF's have the highest internal surface area, often exceeding

6000 m^2/g (see Figure 4).[37] Organic and inorganic chemistry are often treated as separate and distinct fields, but MOFs dispute this notion. Their structure epitomises the beauty of combining these two disciplines. Similar to zeolites, MOF's have primary and secondary building units. Generally, MOF's are composed of metal nodes (or centres) that are bonded together through the use of organic 'linkers' - The 'prototypical' MOF is IRMOF-1 (or MOF-5), and its structure is composed of Zn_4O SBU's that combine into a cage-like porous structure.

With the vast array of metal centres and organic ligands, MOF's have extremely versatile structures, and pore-sizes can be fine-tuned for many applications such as gas storage and separation. Due to their versatility and large surface areas, there is academic interest in using MOFs for carbon capture. As of 2019, over 35,000 MOF structures have been published in the CCDC, and therefore, a thorough review will not be conducted here. For a more detailed reference please see work by Ding et al.[38] Numerous studies, however, have investigated the use of MOFs in carbon capture. A notable characteristic of MOFs used in carbon capture is the incorporation of heteroatoms into the molecular framework. Atoms with high polarities and nucleophillic natures, such as nitrogen, have shown to improve interactions with CO_2.[39] One such is example is the use of Zn(btz), which has two non-coordinating nitrogen atoms as part of the organic linker; the resulting structure showed CO_2 uptakes of 18 wt% at ambient conditions. Recent work by Zhang *et al* showed that the incorporation of Lewis basic sites into MOF structures can drastically improve adsorption and CO_2 selectivity

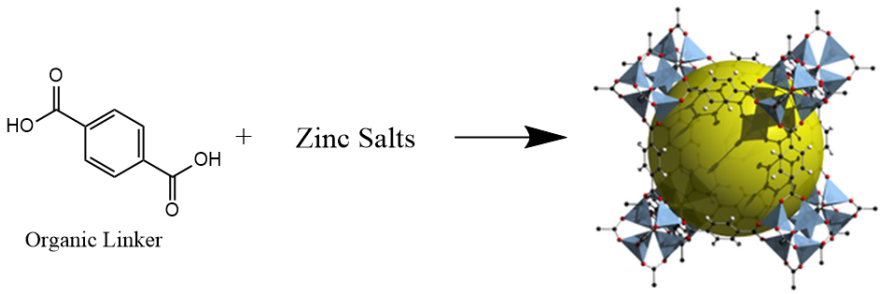

Figure 5: Diagram showing a basic synthetic route to IRMOF-1, one of the best-known and well studied MOFs. IRMOF-1 has a maximum BET surface area of 2517 m^2/g.

.

- this is rationalised by the interaction of localised nitrogen dipoles with the quadrupole moments of CO_2.[40] Despite high surface areas, MOFs do suffer from a number of issues that would affect the adsorption of CO_2 from flue gas. They can be extremely sensitive to water and moist environments, and current MOF structures that show resistance to water (within a carbon capture setting), fall short of other available materials.[39] Further to this, most studies examine MOF capacities at low temperatures such as 298 K. This is an issue, due to most commercial processes desiring CO_2 removal from a high temperature flue gas - typically between 343 and 363 K.

2.3.3 Porous Carbons

Porous carbons come in many shapes and sizes. They can be categorised into low-cost pyrogenic carbons, activated carbons, and carbon nanomaterials such as graphene and nanotubes. They are typically amorphous materials that have a wide-range of tunable pore sizes. The majority of these materials are derived from the pyrolysis of biomass, such as olive stones, raw bamboo and cellulosic materials.[41]

Of all these material types, activated carbons (AC's) have been extensively researched for use in carbon capture. A number of factors are important to consider when choosing the type of AC: the biomass type used in production, conditions under which activation occurs, and the use and incorporation of solvents. Numerous studies have been conducted looking at adsorption capacities

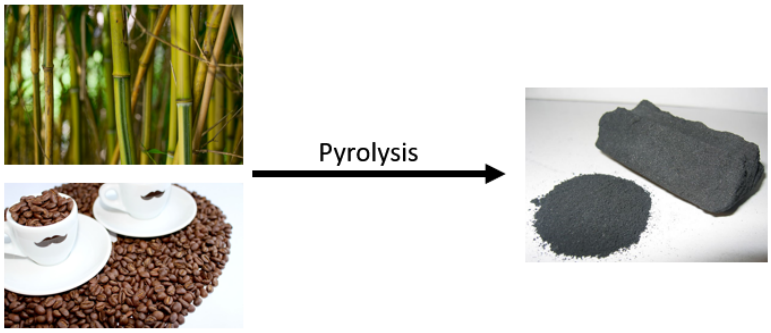

Figure 6: A variety of different biomass types can be used to produce porous carbons. Bamboo and coffee grounds are two examples of materials that can be pyrolysed to produce activated carbons.

for activated carbons - the literature shows that at temperatures of 273 K and a pressure of 1 bar, CO_2 uptakes range from 2.8 - 8.6 mmol/g. Furthermore, at 298 K and 1 bar, uptake values range from 1.5 - 4.8 mmol/g.[42] One stand-out group of AC's are the amine-impregnated adsorbents. Some commonly used amines for functionalizing ACs include: diethylenetriamine, pentaethylenehexamine, tetraethylenepentamine, and polyethylenimines. Functionalising the surface with amine substituents can enable high adsorption capacities and desirable regeneration properties. Moreover, amine-impregnated AC's can even be used in low-pressure applications, and show high tolerances to water impurities; permitting the humidity isn't too high, studies show that moisture can even improve the uptake of CO_2.[43]

There are many challenges facing the use of solid adsorbents for carbon capture. Many materials show good performance in laboratory studies at lower temperatures, but may show reduced capacities and selectivities within an industrial setting. Moreover, costs of adsorbent production and costs of regeneration are other factors to consider - particularly when considering the application of these technologies in developing countries.

It is clear from a survey of the literature, that physisorptive materials have a large role to play in carbon capture. Nonetheless, no single material meets the criteria for a 'perfect' adsorbent, and it is apparent that materials should be selected on a case-by-case basis.

2.4 Crystalline Urea: A Novel Material for Carbon Capture?

After reviewing the literature on solid-state adsorbents in carbon capture, one theme was apparent throughout: the incorporation of Lewis basic sites, particularly amines, will typically improve the adsorption performance in a variety of materials. Urea is a molecule that shows this type of desirable functionality in its chemical structure (see Figure 7). Urea was first discovered in 1838 by Friedrich Wohler, and was single-handedly responsible for the creation of synthetic organic chemistry as a field. Pure crystalline urea is a white, odourless

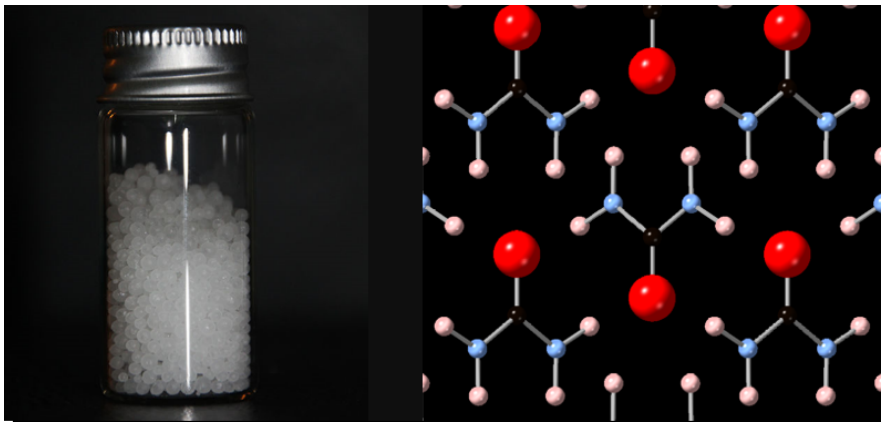

Figure 7: (i) White crystalline urea in a sample vial (ii) Phase I molecular crystal structure of urea. Oxygen atoms are shown in red, nitrogen atoms are shown in blue, and hydrogen atoms are shown in white.

solid with a melting point of 132 - 135 °C, and a density of 1.34 g/cm^3. Moreover, it is well known for its role in biochemical and metabolic processes, and it has been shown that the human body produces approximately 25 g of urea per day.[44] Urea is the textbook example of a molecular crystal - over the last decade or so, the use and application of molecular crystals has gained much attention. They have previously been used in applications such as pharmaceuticals, OLED devices, fertilizers and inks. A molecular crystal is a solid-state material that is composed of individual molecules - the packing arrangement of these molecular crystals is determined by weak, short- and long- range interactions such as Van de Waals forces, dipole-dipole interactions, hydrogen bonding and quadrupole moments.[45]

It has been identified that urea shows the pre-requisite chemical functionality to perform as an adsorbent in post-combustion carbon capture. It is clear that urea shows similar functionality to other sorbents used commercially - monoethanolamine is the most commonly used absorbent for post-combustion carbon capture, whilst ethylenimine is often used to functionalise activated carbons (see Figure 8).[43,46] Despite this observation, there are many factors to consider when designing new adsorbents. Adsorbent availability, sustainability, and costs are a few of the key considerations. Due to its use in the production of fertiliser, large amounts of urea is manufactured every year. At the end of 2016, $>$ 174 million tonnes of urea had been produced across the globe.[47] This indicates that the long-term availability of urea should not be an issue.

Furthermore, with a relatively cheap cost attached to urea, a few key criteria for commercial adsorbents have already been met. To further examine the use of urea for carbon capture, is is necessary to understand and assess the physisorptive capacity and selectivity towards CO_2. To achieve this, *in silico* isotherm simulations offer a low-cost method for predicting if urea is a suitable candidate material for next-generation carbon capture. As of 2019, no studies have previously investigated crystalline urea as a potential gas adsorbent.

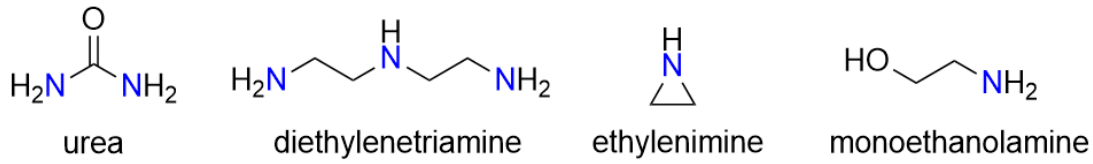

Figure 8: Molecular structures of urea, diethylenetriamine, ethylenimine and monoethanolamine. The structure of urea shows similar functionality to other molecules used in carbon capture. Lewis basic sites are labelled blue.

2.5 Computational Simulations: How to Simulate Adsorption?

Computational simulations offer a fast, low-cost method for assessing the adsorption properties of crystalline materials. For adsorption applications, a variety of useful metrics can be obtained from molecular simulations: e.g. adsorption capacities and interaction energies. Experimental adsorption studies can often be extremely time consuming, and molecular simulations offer a faster route to obtaining adsorption isotherms. Furthermore, when measuring experimental isotherms, it can be difficult to know if your system has reached the associated equilibrium pressure; this issue can be circumnavigated through molecular simulation.[48] Experiment and theory are often considered distinct entities, but it is worth noting here, the importance of combining experimental and computational data. A symbiotic relationship exists between the two data types and much can be learned from a combined approach. This section will introduce the most common approach to simulating adsorption isotherms.

One of the best known approaches for simulating adsorption isotherms is Monte Carlo. These methods can be traced back to early 18th century, where prominent

French scientist Georges Comte de Buffon asked the question "Do random events ever lead to concrete results?". The idea of using random patterns to understand macroscopic phenomena was ground-breaking. Nowadays, Monte Carlo is a heavily used mathematical tool for simulating stochastic systems, and processes where experimentation is particularly time consuming.[49] For applications to adsorption equilibria, the Grand Canonical Monte Carlo (GCMC) approach is most common, and is formulated on the idea of importance sampling. When measuring experimental isotherms, the adsorbed gas is at equilibrium with the reservoir gas, and a fixed temperature (T), volume (V) and chemical potential (μ) is mandatory. The Grand Canonical ensemble, or 'μVT' ensemble, can simulate these conditions and is specifically used for molecular processes that require a fixed temperature, volume and chemical potential - on the other hand, the number of gas molecules is not kept constant and is allowed to fluctuate. The number of simulated gas molecules is allowed to change through a variety of trial moves. For example, insertion, deletion, rotation and translation are the four move types associated with a single-component isotherm.[50] After each move type, the system energy is calculated, and a decision is then made on whether to accept or reject the change - more information on this method, and how the system energy is calculated, is given in chapter 4 of this report.

The literature shows many computational studies that investigate the adsorption of CO_2 on solid adsorbents. One such example is a study by Liu and Wilcox, where they simulated the adsorption of CO_2 in micro-porous and meso-porous carbons at temperatures and pressures associated with underground coal.[51] They used density functional theory to better understand the electronic properties of functionalised carbon surfaces, followed by GCMC simulations at a variety of temperatures and pressures. From a review of the literature, one thing is apparent - irrespective of the adsorbent and adsorbate, a 'standard' work-flow exists for the simulation of adsorption isotherms. Typically, higher level quantum mechanical calculations are performed to calculate partial charges and optimise the adsorbent structure, followed by GCMC simulations at a range of different temperatures and pressures.[51–54] Therefore, this methodology shall be applied in this work to examine the adsorption of CO_2 on different surfaces of crystalline urea.

Chapter 3

Aims and Objectives

Broadly speaking, the aim of this project is to use a variety of computational methods to assess if urea is a suitable material for physisorptive carbon capture.

This project attempts to answer two key questions:

1. What are the most common crystal surfaces found in urea, and how strong is the binding energy between these surfaces and CO_2? This question intends to predict if the process is feasible at the experimental level. If the interaction between a urea framework and CO_2 is too low, minimal adsorption will occur. Furthermore, if the interaction is too high, the recovery of CO_2 may become too energy intensive.

2. Estimate the potential capacity of urea for CO_2. If the capacity is too low, large volumes of urea would be needed for sufficient adsorption, therefore leading to greater costs.

Depending on adsorbent properties, embedding crystalline urea into a cellulose-based matrix is of particular interest in the long term. However, this project hopes to better understand if **pure** crystalline urea is a strong candidate material for a novel, sustainable, energy efficient, next-generation bio-based carbon capture technology.

Chapter 4

Computational Methods

4.1 Crystal Structures

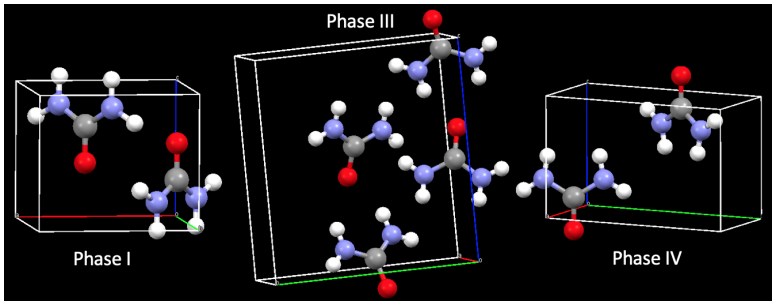

Figure 9: Three experimentally derived unit cells of urea, obtained from the Cambridge Crystallographic Data Centre.

Molecular crystals, such as urea, typically have a variety of low-energy structures. Very few of these structures, however, can be confirmed through experimental methods. Urea has three experimentally derived phases in the literature, and in this work, each phase will be computationally examined for the adsorption of CO_2 (see Figure 9). The three phases are: phase I (under ambient condition), phase III (high-pressure phase), and phase IV (high-pressure phase).[55,56] For each phase of urea, the Crystallographic Information Files (CIF) were obtained from the Cambridge Crystallographic Data Centre (CCDC). The unit cell information is listed below in Table 1:

	Space Group	*Atom No*	*x (Å)*	*y (Å)*	*z (Å)*	*a*	*b*	*c*	*Cell Volume*
Phase I	$P42_1m$	16	5.582	5.582	4.686	90	90	90	146.01
Phase III	$P2_12_12_1$	32	3.420	8.145	8.758	90	90	90	243.97
Phase IV	$P2_12_12$	16	3.408	4.648	7.363	90	90	90	116.63

Table 1: Unit cell parameters for the three known phases of urea.

4.2 Crystal Face Prediction

Crystal face predictions were performed using Mercury Version 3.10.1, a crystallographic software developed by the CCDC.[57] In order to simulate the adsorption of CO_2 on urea, it is necessary to understand and predict which surfaces will be predominately exposed at the crystal-air interface. In order to achieve this, Bravais-Friedel-Donnay-Harker (BFDH) theory was used to predict the relevant crystal faces. This theory was built over many years; Bravais (1866), Friedel (1906), Donnay and Harker (1937) proposed the idea of using lattice geometries to simulate the morphology of crystals. The theory can be formally summarised as such: 'taking into account sub-multiples of the inter-planar spacing due to space group symmetry, the most important crystallographic forms will have the greatest inter-planar spacings'.[58] In a less verbose manner, crystal faces with larger inter-planar distances will grow faster. Therefore, if the crystal space group is known, along with unit cell dimensions and extinction conditions, the predominant morphologies can be predicted.

It is important to note that BFDH theory does show some weaknesses. The crystal framework is only *structurally* considered, and no attention is paid to atomic types, bond types (and strength), and atomic partial charges. These factors have a clear role to play in the the kinetics of crystal growth, and therefore, improved models may exist in place of BFDH theory.[59] Despite this, BFDH theory is a well known and well accepted theory. Also, it is extremely fast and computationally efficient. For these reasons, it was our chosen methodology.

4.3 Density Functional Theory

4.3.1 Introduction

Within the realms of quantum chemistry, we are concerned with trying to solve the time independent, non-relativistic Schrödinger equation as shown in equation (1) below:

$$\hat{H}\Psi = E\Psi \tag{1}$$

Where $\hat{H}$ is the Hamiltonian operator, Ψ is the wavefunction and E is the energy of the system. In compact notation, the many-body Hamiltonian can be written as a sum of five terms:

$$\hat{H} = \hat{T}_N(R) + \hat{T}_e(r) + \hat{V}_{eN}(R,r) + \hat{V}_{NN} + \hat{V}_{ee} \tag{2}$$

Where $\hat{T}_N(R)$ is the kinetic energy of the nuclei, $\hat{T}_e(r)$ is the kinetic energy of the electrons, and the V terms describe the electron-nuclear, nuclear-nuclear and electron-electron potential energies (in the order shown above). DFT is an electronic structure theory where the Born-Oppenheimer (BO) approximation has been invoked, indicating that nuclear and electronic motion has been decoupled. Therefore, for a given nuclear configuration, this leads to the 'clamped nuclei' electronic Hamiltonian as below:

$$\hat{H}_e = \hat{T}_e(r) + \hat{V}_{eN}(R,r) + \hat{V}_{ee} = -\frac{\hbar}{2m_e}\sum_i \nabla_i^2 - \sum_{A,i}\frac{Z_A e^2}{4\pi\epsilon_o r_{iA}} + \sum_{i>j}\frac{e^2}{4\pi\epsilon_o r_{ij}} \tag{3}$$

The BO approximation states that due to the drastic difference in mass between nuclei and electrons, the nuclei can be treated as stationary when considering electronic motion. The outcome of this approximation results in the nuclei being part of an external potential, thus allowing redefinition of the electronic Hamiltonian:

$$\hat{H}_e = \hat{T}_e(r) + V_{ext}(R) + \hat{V}_{ee} \tag{4}$$

The many-body wavefunction shown in equation (1) is dependent on 4N coordinates, where N is the number of electrons in the system. Therefore, as the number of electrons increase, the 4N dependency leads to an exponential increase in wavefunction complexity. The result of this complexity is a time-consuming,

computationally expensive calculation. Density functional theory tries to simplify the problem of solving the many-body Schrödinger equation - in DFT, the electron density is defined as the square of the wavefunction integrated over N-1 coordinates:

$$\rho(r_i) = \int |\Psi(r_1, r_2 ... r_i)|^2 dr_2, dr_3 ... dr_i \tag{5}$$

The electron spin density is therefore only dependent on three coordinates, thus reducing the dimensionality of the problem. The fundamental foundation of DFT comes from an idea put forward by Hohenberg and Kohn. This idea stated: 'the ground state energy of a system can be completely determined by the ground state electron density'.[60] To understand this intuitively, E.B. Wilson proposed three key ideas that explain why there is a one-to-one correspondence between the ground-state energy and the electron density:

1. Cusps in the electron density define the position of the nuclei.
2. The heights of the cusps correspond to the charge on the nuclei.
3. The electron density will integrate to the total number of electrons in the system.

The entirety of DFT is built on two theorems as proposed by Hohenberg and Kohn. To briefly summarise these two theorems, the **first** states: '*The external potential $V_{ext}(r)$, and hence the total energy, is a unique functional of the electron density*'. The **second** theorem states *'The ground state can be obtained variationally: the density that minimises the total energy is the true ground state density'.*[61] Early attempts at building models (that use the electron density to account for all energy terms), such as the Thomas-Fermi model, were not particularly accurate, and traditional wavefunction based approaches were preferred. It was only when Kohn and Sham introduced an orbital approximation to DFT, such as that in Hartree-Fock theory, that DFT became popular in use.

4.3.2 Kohn-Sham DFT

The use of DFT in computational chemistry was popularised by the introduction of orbitals into the mathematical framework. First and foremost, KS-DFT is concerned with using an orbital approach to minimise the system energy with

respect to the electron density. The orbital basis-sets consist of either Gaussian Type Orbitals (GTO's), plane waves, or a combination of the two - plane wave approaches are particularly used in the physics of periodic systems such as crystals. Plane wave approaches are derived from Bloch's theorem which will not be discussed in this work - for more information, please see work by Dobardžić *et al.*[62] There is, however, a downside to adopting an orbital approach. The introduction of orbitals increases the dimensionality of the problem; 3N dependency is introduced to the equations, replacing the simplistic N dependency seen in orbital-free methods.

The fundamental problem with previously derived models, such as the Thomas-Fermi model, related to the calculation of kinetic energy (KE). Kohn and Sham proposed the idea of separating the KE functional into two parts: one which could be exactly calculated, and the other which would need to be approximate. Similarities are easily noted between Hartree-Fock (HF) theory and DFT, with almost identical expressions appearing in the HF electronic Hamiltonian and the DFT energy expression as below:

$$E_{DFT} = T_s[\rho] + E_{ne}[\rho] + J[\rho] + E_{XC}[\rho] \tag{6}$$

The key to Kohn-Sham DFT is to calculate the kinetic energy in a 'mean-field' approach, similar to that in Hartree-Fock theory.[63] This results in a pseudoeigenvalue equation as below:

$$\hat{h}_i \chi_i = \epsilon_i \chi_i \tag{7}$$

Where $\hat{h}_i$ is the one-electron Kohn-Sham operator and χ_i are the chosen orbitals. In reality, the electrons are both correlated and interacting. Although 99 % of the true system energy will be accounted for by the first three terms in equation (6), accounting for electron correlation is vital in obtaining the final 1 %. The interaction energies that are not taken into account through a mean field approach are treated in the fourth part of equation (6), the exchange-correlation term E_{XC} as below:

$$E_{XC}[\rho] = (T[\rho] - T_s[\rho]) + (E_{ee}[\rho] - J[\rho]) \tag{8}$$

Equation (8) sits at the absolute center of DFT. The first term in equation (8)

represents the correlation energy, whilst the second term describes the exchange energies. Simply put, the first sum accounts for the error that stems from adopting a mean-field approach to calculating the KE, whilst the second sum accounts for the error in treating the electron-electron interactions classically. To briefly summarise, DFT is a methodology used to solve the electronic Schrödinger equation, and has advantages over traditional wavefunction based approaches due to reduced dimensionality. An orbital approach is required for use in computational chemistry, and as a field, DFT is concerned with using and developing innovative functionals that describe the all so important, exchange-correlation term.

4.3.3 Cutoff and Relative Cutoff Values

All DFT calculations were performed using CP2k Version 3.0, a quantum chemistry and solid state physics package that can simulate a variety of systems e.g. liquids, crystals.[64] Specifically, it supports the use of basis sets with a mixed plane-wave and Gaussian approach. CP2k requires the use of a real-space integration grid in order to represent some important functions such as the electron density and product Gaussians. The methodology used in CP2k changes the grid type depending on the product Gaussian type - e.g. a wide, smooth Gaussian will be placed onto a coarser grid than a tall, narrow Gaussian. To ensure a sufficient level of accuracy, it is vital that the correct grid type is chosen throughout the energy minimisation procedure. Moreover, it is simultaneously important to ensure that calculation times are still reasonable. Discretization of the integration grid effects the length of time taken for a calculation to finish; a higher number of 'fine' integration grids leads to longer wall-times.

Throughout this work, the number of grid levels 'NGRIDS' chosen for geometry optimisation calculations was 4. A 'CUTOFF' value also needs to be defined, and this dictates the plane wave cut-off for the finest integration grid. For different grid levels, the respective cutoff is defined by equation (9) below:

$$E^{i}_{CUT} = \frac{E^{1}_{cut}}{\alpha^{(i-1)}} \tag{9}$$

Where α is set to a default value of 3. Once the multi-grids have been defined,

the basis set functions need mapping onto the grids. A relative cut-off value, or 'REL CUTOFF', is set to dictate which Gaussian functions are mapped onto which grid type (coarse or fine). If the relative cut-off value is too low, most product Gaussians will be mapped onto the coarsest grid type, thus leading to inaccurate results. The 'CUTOFF' and 'REL CUTOFF' values were determined for each phase of urea - more specifically, the values were determined for the unit cell of phase I, phase III and phase IV.

In order to determine these parameters, a series of single point energy calculations were carried out. To start, a default relative cut-off value was chosen of 60 Ry. The cut-off value is then systematically changed from a value of 50 to 700 Ry in increments of 50. The single point energy calculations should eventually converge at a specific cut-off value, with this value determining a sufficient level of accuracy to use in future calculations with the respective system. Using the newly established 'CUTOFF' value, the same method was applied to the determine the relative cut-off. In this case, the values were changed from 10 to 100 Ry in increments of 10 Ry. Table 2 shows a list of determined 'CUTOFF' and 'REL CUTOFF' values for the urea systems.

	Phase I	*Phase III*	*Phase IV*
Cutoff	600	600	600
Relative Cutoff	70	80	80

Table 2: Cutoff and Relative Cutoff values for urea unit cells.

4.3.4 Energy Minimisation

Within chemistry, many multi-dimensional problems can be solved by using optimisation methods such as energy minimisation. In computational chemistry, the word 'optimisation' typically means to to find the stationary points of a chosen function - minima and first-order saddle points (transition states) are of particular interest in molecular modelling. Many optimisation techniques are used to scan the potential energy surface (PES) of a system, and aim to find the nearest *local* minimum. Multi-dimensional functions can have many *local* minima, and this relates to one of the key challenges within computational chemistry - to find the *global* minimum for a given system.

Optimization Method

In this work, three unit cells of urea were optimised in an iterative self-consistent field procedure. To speed up convergence of this procedure, Pulay mixing (alternatively called 'Direct Inversion of the Iterative Subspace') was used.[65] This procedure takes a number of trial vectors from the full-dimensional space to aid in solving a smaller set of linear equations within a sub-space.

Naturally, in this work, the energy being minimised is derived from the electron density using DFT. The process of minimisation aims to reduce the unit cell energy E_{UC} as a function of atomic coordinates $\mathrm{r_i}$, thereby reducing the stress on each atom to zero:

$$\frac{\delta E_{UC}}{\delta r_i} = 0 \tag{10}$$

A variety of different optimisation methods exist. First-order and second-order optimizers are available, but only second-order quasi-Newtonian methods were used in this work. The Broyden–Fletcher–Goldfarb–Shanno algorithm was used throughout this work, and is used to solve unconstrained non-linear optimisation problems in an iterative manner.[66] The basic idea of the BFGS algorithm is that energy minima on a potential energy surface are quadratic when making small atomic displacements. Therefore, the energy minima can be completely determined by a Hessian matrix A. That is, a matrix containing the second derivatives of an energy function:

$$(\mathrm{Hess}\, E)_{ij} \equiv \frac{\partial^2 E}{\partial x_i \partial x_j} \tag{11}$$

$$\delta E = \frac{1}{2}(X - X_{min})A(X - X_{min}) \tag{12}$$

Therefore, if A is known, we could immediately move to the minimum. In reality, it is not so simple. The inverse Hessian A^{-1} must be approximated in the first few atomic displacements. The BFGS algorithm was chosen due to it's fast convergence time, combined with being well adapted to the optimisation of molecular geometries.

Basis Set and Exchange-Correlation Functional

The chosen exchange-correlation functional, PBE, sits within the generalised gradient approximation (GGA). It is a well known functional for it's general applicability to molecular systems, and gives relatively accurate results for it's position on Jacob's ladder (a grading system used to rate the accuracy of exchange-correlation functionals in DFT).[67] To improve calculation accuracy and account for dispersion forces, Van de Waals corrections were added to the energy equations. Dispersion interactions governed by the Van de Waals equation are mostly non-local effects, and the PBE functional is built to deal with local interactions. Thus, it cannot independently capture long-range interactions.

The same basis set was used to treat all atoms within the crystalline urea systems. A high-level of theory was used throughout the calculations - a triple-zeta basis set with 2 sets of added polarisation functions was used (TZV2P-MOLOPT).[68] This indicates that three contracted Gaussian functions are used for each orbital, along with the addition of 2 polarisation functions according to the equation below:

$$l = l_{max} + 1 \tag{13}$$

Where l is the orbital angular momentum number of the added polarisation function, and l_{max} is the orbital angular momentum number of the orbital **being** polarised. A review of the literature showed that TZV2P has previously shown excellent accuracy in both gas and condensed phase systems, along with minimising basis-set superposition error.[69] For these reasons, TZV2P-MOLOPT was the chosen basis.

4.4 Slab Creation

In order to simulate adsorption on a crystal surface, slabs must be generated that allow the use of a suitable interaction cut-off value. Computational methods are limited by the number of atoms that can be stored in the system memory, therefore causing the simulation of infinite systems to be computationally infeasible. This begs the question, 'how can we extract macroscopic properties from finite simulations?'; one common solution to this problem is the use

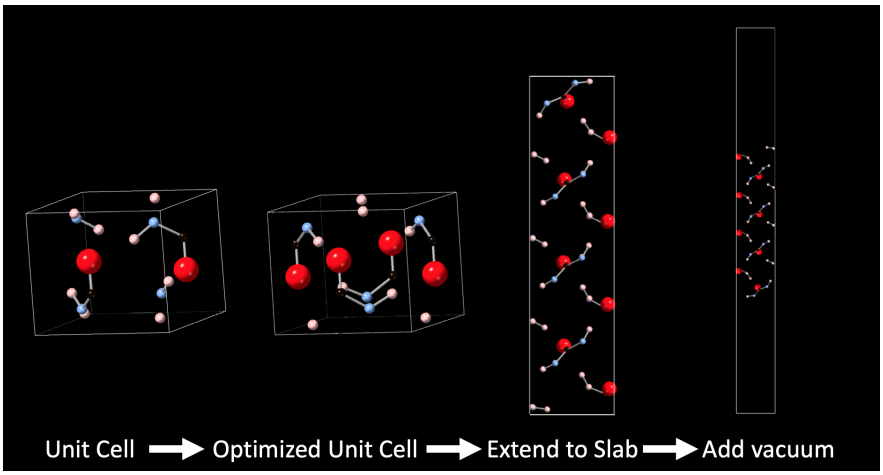

Figure 10: Generalised process for the *in silico* generation of crystalline urea slabs.

of periodic boundary conditions, where the system under study is replicated through space in a periodic array. If an atom or molecule leaves the simulation box, it will re-enter the box (in the same position) through the opposite face, thereby simulating a quasi-infinite system. Further to this, the minimum image convention (MIC) needs to be obeyed: this convention states that the distance between two atoms is taken to be the shortest distance between their periodic images.

The procedure for slab generation remained the same for all crystal surfaces (see Figure 10). Firstly, it was pre-determined that a Lennard-Jones cut-off of 18 Å would be used for all atoms included in the simulations (see section 4.5.3). Therefore, in order to obey the minimum image convention, optimised urea unit cells were extended to a length of 20 Å. Furthermore, crystalline urea is a non-porous material, and would show no adsorption without the introduction of vacuum parallel to the crystal face. For this reason, 15 Å of 'vacuum space' was introduced to either side of the slabs. This ensures that once periodic boundary conditions are introduced, a total vacuum space of 30 Å will sit between periodic images of the crystal surfaces. The distance of 30 Å was chosen to prevent strong interactions between adsorbate molecules and two crystal surfaces simultaneously. Once the slabs were fully generated, density functional theory was used to relax the crystals into the vacuum.

4.5 Monte Carlo Methods

To understand the thermodynamic behaviour of molecular systems, it is necessary to obtain information about their average positions over long time scales. A methodology similar to Monte Carlo is molecular dynamics (MD); MD solves Newton's equations of motion to calculate the evolution of a system over time. The key difference in Monte Carlo is the lack of time integration, with each 'snapshot' of the system being independent on the previous step. As discussed in section 1.5, a number of 'move' types are available in a Monte Carlo simulation. Such as, translation or rotation of an atom (or molecule) within the simulation box. There is, however, an 'acceptance rule' which dictates whether the move, and therefore the next system snapshot, is accepted or rejected. All of these steps form a Markov chain - a mathematical framework whereby the system under study moves from one state to another according to some rule of probability. The strength of Monte Carlo lies in the lack of constraints on different move types; the only constraint is ensuring the correct statistical ensemble is obeyed, which is easily achieved through the use of acceptance rule criteria.

4.5.1 Statistical Ensembles

A key concept that underpins Monte Carlo is that of statistical ensembles. To understand the microscopic nature of a classical system, 6N variables are required. Each particle within the system has three position coordinates and three velocity coordinates, and this collection of terms is defined as a *phase space*. To extract macroscopic quantities such as temperature and pressure, phase-space time averaging is required. In the early 20th century, Gibbs introduced the term 'ensemble', and noted that averaging a set of micro-states (that correspond to the same macro-state e.g. T, P) is equivalent to time-averaging. This equivalence is called the 'ergodic principle'. A variety of statistical ensembles can be used in molecular simulation, and the choice of a particular ensemble is dependent on the physical circumstances. An entire text could be dedicated to the background of statistical thermodynamics, but for the sake of the reader, a brief introduction to the ensembles will be given below.[50]

The microcanonical ensemble, or NVE ensemble is used to simulate the

possible states in a system that has constant energy. The NVE ensemble keeps the number of particles N, the volume V and the energy E constant within the system. This ensembles assigns an equal probability to every system 'snapshot' that lies within an energy range E. Therefore the probability of observing a given state in this ensemble is:

$$P_S = \frac{1}{W} \tag{14}$$

Where P_S is the probability of being in state S, and W is the number of possible microstates within the system. The NVE ensemble is the least used ensemble in practice; the variables kept constant throughout the simulation are difficult to maintain in experimentally realistic scenarios.

The canonical ensemble, or NVT ensemble involves probing the possible microstates of a mechanical system at thermal equilibrium with a heat bath (at constant temperature). Energy is allowed to be exchanged with the heat bath, and therefore, the temperature is the main determinant in the probability distribution of states. The probability of witnessing a given microstate in the canonical ensemble is given by:

$$P_i = \frac{1}{Z} e^{\frac{F-E_i}{k_B T}} \tag{15}$$

Where the partition function is also defined by:

$$Z = \sum_{1}^{N} p_i e^{\frac{-E_i}{k_B T}} \tag{16}$$

In the equations above, E_i is the energy of microstate i, k_B is the Boltzmann constant, p_i is the probability of state i, and F is the free energy of the ensemble. The free energy F of a given ensemble is kept constant throughout, but changing N, V or T will lead to a different probability distribution and therefore a different system F. The canonical ensemble is one of the most practically useful ensembles; systems that exist at thermal equilibrium with their external environment are often considered in experimental set-ups.

The Grand Canonical Ensemble has been used substantially in this work, and will be discussed in greater depth in the next section.

4.5.2 Simulation of Adsorption: Grand Canonical Monte Carlo (GCMC)

Theory Introduction

In this work, adsorption simulations were performed under conditions imposed by the grand canonical ensemble. This allows the user to predict the amount of material adsorbed as a function of both temperature and pressure. In GCMC, the mechanical system under study is in thermodynamic equilibrium with a reservoir, and the chemical potential, volume, and temperature are kept constant throughout. Equilibrium conditions are reached by setting the chemical potential of the reservoir and simulation box to be equal constants. Hence, the grand canonical ensemble is often termed the μVT ensemble. The number of particles in the simulation is not kept constant and is allowed to change; in a sense, the system is 'open'. In this work, the reservoir contains either CO_2, N_2 or a combination of the two. These molecules will be inserted, deleted, translated, rotated, or replaced in vacuum space adjacent to the crystal surfaces of urea. Figure 11 shows a general formula for a GCMC simulation, including the 'fictitious' reservoir that allows the number of particles to change.

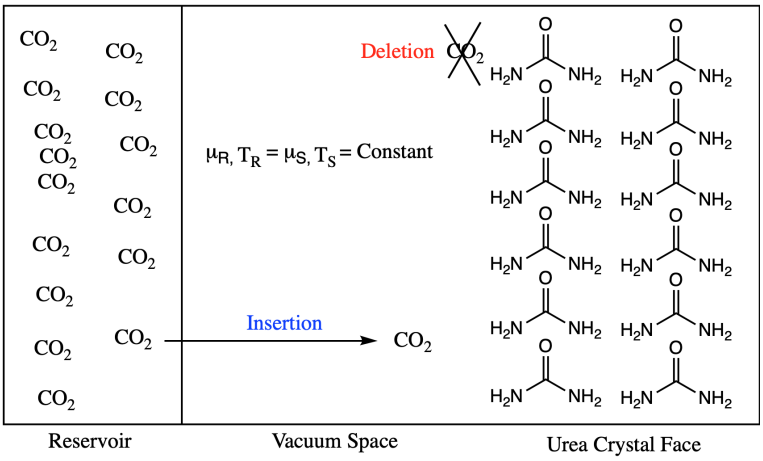

Figure 11: Representation of a Grand Canonical Monte Carlo simulation. The reservoir contains carbon dioxide molecules that can be inserted, rotated, translated, or deleted in the simulation box. The chemical potential and temperature are set constant.

As shown in section 4.4.1, the partition function is defined by summing over all possible microstates in the system, multiplied by the probability of that state.[70]

The partition function for the grand canonical ensemble is defined as below:

$$Z(\mu, V, T) = \sum_{N=0}^{\infty} \frac{V^N e^{\beta\mu N}}{\Lambda^{3N} N!} \int e^{-\beta U(s^N;h)} d^N \mathbf{s} \tag{17}$$

Where V is the volume, N is the number of particles, β is the Boltzmann factor and μ is the chemical potential.[50] Furthermore, the probability prescribed to a particular configuration is shown below:

$$P(s^N, V) \propto \frac{V^N e^{\beta\mu N}}{\Lambda^{3N} N!} e^{-\beta U(s^N;h)} \tag{18}$$

Not all changes or moves performed on the system will be accepted. Whether a move is accepted or rejected is dependent on acceptance rules used in the Monte Carlo simulation. In this work, the Metropolis sampling algorithm was used as the acceptance rule.[71] The acceptance rule for displacement of a particle (translation or rotation) is:

$$acc(s \to s') = min(1, e^{-\beta[\kappa(s'^N) - \kappa(s^N)]}) \tag{19}$$

Where κ is the potential energy function and s defines the system state. Furthermore, for insertion or deletion of a particle, the acceptance rule is as shown below:

$$acc(N \to N+1) = min[1, \frac{V}{\Lambda^3 (N+1)} e^{\beta[\mu - \kappa(N+1) + \kappa(N)]}] \tag{20}$$

According to the Metropolis algorithm, if the energy of a new state is lower than the energy of the previous state, the change is automatically accepted. If the energy is higher, a random number between 0 and 1 is generated, and if $-\Delta\kappa$ is greater than the randomly generated number, the move is accepted.

4.5.3 Potential Models

In order to utilise Monte Carlo for adsorption, and to make the acceptance rules applicable, the system energy must be calculated. To calculate the energy, it is first necessary to define the interactions between atoms and molecules within the simulation box.

Van de Waals Potential

To account for van de Waals dispersion interactions, a 12-6 Lennard-Jones potential was used:

$$V_{vdw}(r) = 4\epsilon[(\frac{\sigma}{r})^{12} - (\frac{\sigma}{r})^{6}] \tag{21}$$

Where ϵ corresponds to the well-depth (and therefore interaction strength), and σ corresponds to the large-sphere diameter which relates to atom size. Force field derived parameters are traditionally used for σ and ϵ - however, these are typically self-interacting parameters and a 'mixing rule' is required to adequately describe the interaction between an atom i and an atom j. The Lorentz-Berthelot mixing rules were used throughout this work, as shown below in equations 22 and 23:

$$\epsilon_{ij} = \sqrt{\epsilon_i \epsilon j} \tag{22}$$

$$\sigma_{ij} = \frac{\sigma_i + \sigma_j}{2} \tag{23}$$

To model carbon dioxide and nitrogen, ϵ and σ values were derived from the TRaPPE force field and included in the Lorentz-Berthelot mixing rules (see Table 3).[72] Furthermore, to model the crystalline urea framework, ϵ and σ values were derived from the Universal Force Field (UFF). Throughout this work, to improve computational efficiency, a cut-off value of 18 Å for the van de Waals interactions was introduced to the energy equations. A number of factors are important to consider when choosing a Lennard-Jones cut-off, but the theoretical details of this will not be discussed in this work - for more details, please see work by Siperstein *et al.*[73]

	Force Field	σ	ϵ
Carbon (CO_2)	TraPPE	2.800	27.000
Oxygen (CO_2)	TraPPE	3.050	79.000
Nitrogen (N_2)	TraPPE	3.310	36.000
Carbon (Urea)	UFF	3.851	52.790
Hydrogen (Urea)	UFF	2.886	22.122
Nitrogen (Urea)	UFF	3.660	34.691
Oxygen (Urea)	UFF	3.500	30.166

Table 3: Force field parameters used in the Lorentz-Berthelot mixing rules for this study.

Coulomb Potential

To describe the electrostatic interactions between atoms i and j, a coulomb potential is defined as below:

$$U_{coul} = \frac{1}{4\pi\epsilon_o} \sum_{i<j} \frac{q_i q_j}{|r_i - r_j|} \tag{24}$$

Where q represents point charges i and j, ϵ is the permittivity of vacuum, r_i describes the coordinates of atom i, and r_j describes the coordinates of atom j. For a system with a defined number of atoms, this sum can be completely evaluated and the energy directly calculated. However, in the case of an infinite system, mathematical tricks must be utilised to aid in energy convergence. In this work, the Wolf summation method was used to evaluate the Coulombic potential between interacting atoms.[50] In order to fully evaluate the coulombic potential between one point charge and all other charges in the system, an infinite distance should be considered. In reality, infinite distances can not be considered computationally and truncation of the distance is necessary. Wolf proposed the idea of adding a truncation sphere of radius R_c to each point charge - therefore, only interactions that lie within the truncation sphere are considered. Now, according to the rules of electrostatics, the interaction between an atom with charge q_i and a charged surface of radius R_c is:

$$E_i^{neutr}(R_c) \approx \frac{q_i \Delta q_i(R_c)}{R_c} \tag{25}$$

We can also define $\Delta q_i(R_c)$ as the charge of a sphere centred on atom j:

$$\Delta q_i(R_c) = \sum_{j, r_{ij} \leqslant R_c} q_j \tag{26}$$

And thus, according to Wolf summation, the energy is calculated as such:

$$E_i(R_c) = \sum_{j \neq i, r_{ij} < R_c} \frac{q_i q_j}{r_{ij}} - \frac{q_i \Delta q_i(R_c)}{R_c} \tag{27}$$

Another common method for calculating charges is Ewald summation, which utilises reciprocal space terms that are ignored in Wolf summation. Despite

widespread success of both methods, Wolf summation is faster and more computationally efficient than Ewald, and was therefore used for all simulations in this work.[74]

4.5.4 Absolute/Excess Uptake

In experimental adsorption isotherms, it is the *excess* uptake that is measured. However, adsorption isotherms derived from molecular simulation report the *absolute* uptake values. Absolute uptake is defined as the total number of particles in the simulation free-space, whereas excess uptake only considers the adsorbed atoms/molecules that are interacting with a framework in question.[75] Equation 28 shows how to calculate the excess number of molecules:

$$n_{ex} = n_{abs} - V_g \rho_g \tag{28}$$

Where n_{ex} is the number of excess molecules, n_{abs} is the absolute number of molecules, V_g is the volume of vacuum free space and ρ_g is the molar bulk density of the gas phase. The molar bulk density of the adsorbate is calculated using the Peng-Robinson equation of state, whilst the volume of vacuum free space is determined using the second virial coefficient as described previously by Monson and Myers.[76]

4.5.5 Simulation Details

For Monte Carlo simulations, phase I and phase IV urea were investigated. Throughout this work, MuSIC (Multi-purpose Simulation Code) was used to obtain the adsorption isotherms, and in total, three different sets of simulations were performed:

1. Single component CO_2 isotherms
2. Single component N_2 isotherms
3. Multi component CO_2 / N_2 isotherms

Naturally, to probe the performance of crystalline urea as a carbon capture

material, CO_2 isotherms were assessed. Furthermore, the largest fraction of combusted flue gas consists of un-combusted nitrogen gas, and therefore both single-component N_2 and mixed-component isotherms were assessed to examine CO_2 selectivity.

In order to simulate adsorption isotherms, the simulation settings need to be defined. All simulations were carried out at both 298 K and 310 K, and at discrete pressures ranging from 1 - 50 bar. At each pressure, 10,000,000 steps were simulated for CO_2 calculations, whilst 5,000,000 steps were simulated for N_2 due to faster equilibration. Equal weightings were applied to all move types.

Chapter 5

Results and Discussion

5.1 Crystal Surface Energies

5.1.1 Urea Unit Cells

The unit cell energies for phase I, phase III and phase IV of urea were optimised using density functional theory. The energy of the unit cells can be seen below in Table 4:

	Phase I	*Phase III*	*Phase IV*
Energy (Ha)	- 88.1377010	- 176.1155358	- 88.02494611
Energy (eV)/molecule of urea)	- 1199.175076	- 1198.087528	- 1197.640965

Table 4: Unit cell energies derived from density functional theory.

The relative energies above give an indication to the stability of each crystal morphology. The values are intuitive, considering the conditions under which each phase of urea is found. The lowest energy unit cell is found in phase I of urea - this phase is very stable under ambient conditions, thus in agreement with the relative energies. Phase III is only found at pressures above 0.48 GPa, whilst phase IV is only found above 2.8 GPa. These high-pressure unit cells should typically show higher energies (and therefore less stability) when compared to ambient-phase urea.[55]

5.1.2 Slab Energies

In this work, surface energies were calculated using a standard slab model.[77] This slab model involved generating a supercell that exposed the surface of interest, followed by inserting vacuum perpendicular to the crystal face. Surface energies were calculated according to equation 29 below:

$$E_{Surf} = \frac{E_{slab} - E_{bulk} * n_{slab}}{2 * A_{slab}} \tag{29}$$

Where E_{slab} is the absolute slab energy, E_{bulk} is the energy of the bulk material per atom, n_{slab} is the number of atoms in the slab, and A_{slab} is the surface area of the face in question. Table 5 shows the surface energies and relevant parameters for its calculation:

	Phase I (100)	***Phase I (001)***	***Phase IV (010)***
Energy of Bulk (Ha)	- 88.1377010	- 176.1155358	- 88.02494611
Energy of Slab (Ha)	- 1199.175076	- 1198.087528	- 1197.640965
Number of Atoms (Bulk)	16	32	16
Number of Atoms (Slab)	64	72	48
Surface Energy (J/m^2)	- 0.0575	- 2.2658	- 0.9440

Table 5: DFT-derived surface energies calculated for phase I and phase IV of urea.

According to its definition, the surface energy is the amount of energy required to separate a bulk solid into two pieces at a specific crystallographic face. The results showed that the (100) face in phase I has the highest relative surface energy, whilst the (001) face has the lowest. Also, the (010) face in phase IV sits approximately between the two values observed in phase I. In theory, a higher surface energy infers stronger molecular interactions at the surface; however, the magnitude of these values is difficult to establish due to errors made with the calculation of bulk crystal energy.

The absence of phase III in Table 5 is very apparent. Despite changing the type of optimizer (e.g. BFGS, CG), the slab deriving from phase III would not converge to an energy minima. This is hypothesised to occur due to the intermediate nature of phase III. To further corroborate this result, the existence of its experimental structure still remains a mystery in literature.[55] Further to this, the most striking

feature in Table 5 is that all surface energies are negative. For all stable, solid materials an input of energy is required to form a surface; therefore, all single component surfaces should have a positive surface energy.[78] The negative surface energies can be attributed to the inaccurate calculation of bulk energy; in order to obtain a true bulk energy, the system should be simulated at a number of different volumes. In other words, the energy should be calculated as a function of system size until convergence occurs. A high level of theory was chosen for the energy minimisations, and therefore, the unit cells were treated as the 'bulk' system in this work. This explains the erroneous surface energies, and in retrospect, further calculations should be performed to obtain a completely converged bulk crystal energy.

5.2 Adsorption Isotherms

5.2.1 Adsorption on Phase I Urea

Single component CO_2 isotherms were calculated and obtained for the (100) and (001) surfaces of phase I urea. Simulation results readily showed that (001) shows substantially more adsorption than (100) (see Figure 12). This therefore infers that CO_2 has greater affinity for the (001) surface. At 298 K and 1 bar, the (100) surface showed an absolute adsorption capacity of 0.11 mmol/g, whilst the (001) surface showed a value of 0.29 mmol/g. At these conditions, the (001) surface shows approximately 3 times the adsorption capacity than the (100) surface. Conventional amine scrubbing plants operate with flue gas at a pressure of 1 bar; therefore, predicting the adsorption capacity at this pressure is important for assessing new materials for carbon capture.[19] Furthermore, the interaction energies E_{int} can be examined to understand the strength of the adsorbent-adsorbate interactions. At ambient conditions, the (001) surface showed stronger interactions with CO_2, with an E_{int} value of - 9.15 kJ/mol, compared to the observed value of - 7.58 kJ/mol for the (100) surface.

To further examine the phase I isotherms, higher pressure points should be considered. At 298 K and 45 bar, the (100) surface shows an excess adsorption capacity of 3.27 mmol/g, whilst the (001) surface showed a value of 11.65 mmol/g. From the results discussed above, it is clear that the (100) surface shows relatively

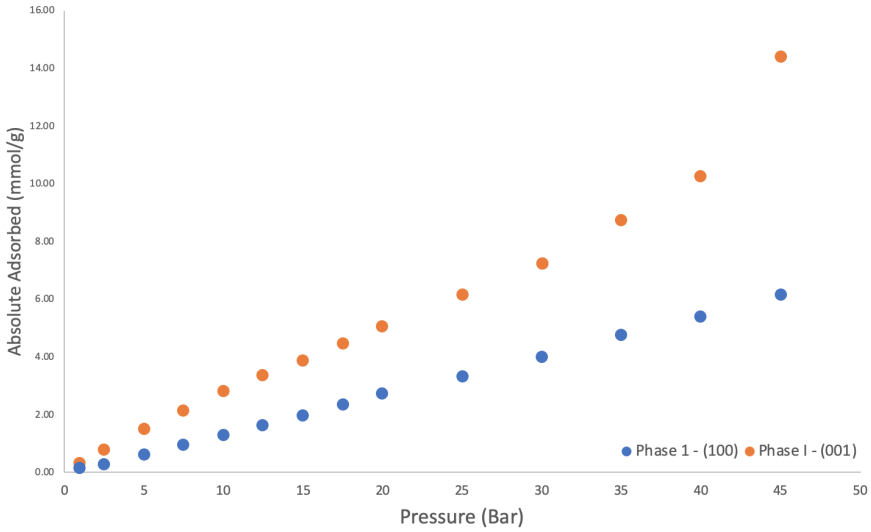

Figure 12: Absolute adsorption capacities at 298 K for the (100) and (001) surfaces of phase I urea.

poor adsorption of CO_2 when compared to the (001) surface. This drastic difference in adsorption capacity can readily be explained with some elementary chemistry and a visual inspection of the surfaces; Figure 13 shows a top-down view of the two surfaces in question. On the (001) surface, the nucleophillic amine groups are coming out of the page and are readily exposed at the crystal-vacuum interface. However, the (100) surface has flat urea molecules in the plane of the paper, meaning that less reactive amines groups are exposed at the interface. The author hypothesises that the (001) surface demonstrates a stronger interaction between the nucleophillic amine groups in urea and the electrophillic carbons in CO_2.

At first glance, it may appear that the adsorption capacity of (001) is relatively high at 45 bar. Despite this, maintaining a balance between interaction strength and adsorption capacity is vital to a successful adsorbent. The results showed that as the simulation pressure increased, the dominant non-coulombic interaction energies also decrease (become less negative). At 45 bar, the interaction energy drops to around - 3.7 kJ/mol; a very weak interaction between CO_2 and the crystal framework. Prior to functionalisation, activated carbon adsorbents show interaction energies ranging from - 25 to - 40 kJ/mol. Moreover, interaction energies ranging from - 40 to - 60 kJ/mol can readily be achieved

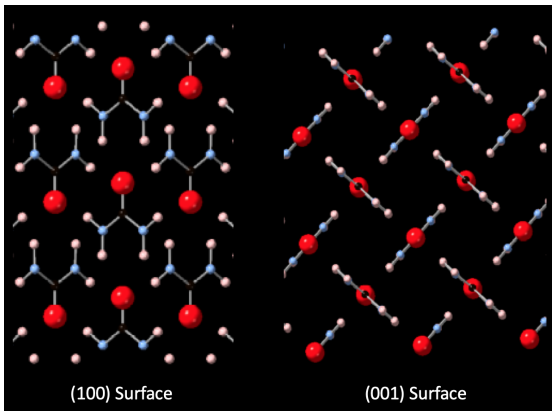

Figure 13: Top-down view of (100) and (001) surfaces of urea. Amine functionality can be observed coming out of the page in (001).

post-functionalisation.[25] Throughout all simulations, the strongest interaction energy observed was ≈ - 10 kJ/mol. If interaction energy largely governs the adsorption properties of a material, it is unlikely that crystalline urea could compete with common adsorbents on the market e.g. zeolites and activated carbons.

5.2.2 Adsorption on Phase IV urea

Adsorption isotherms were only obtained for a single crystal surface of phase IV. Adsorption on (010) was simulated, and the results showed intermediate performance - an adsorption capacity somewhere between the two surfaces in

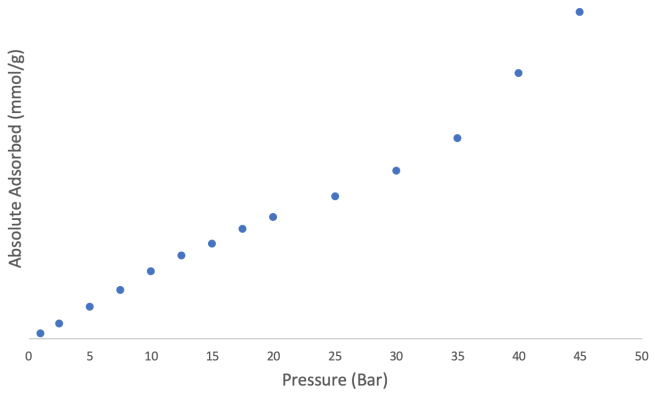

Figure 14: Adsorption isotherm for the (010) surface at 298 K.

phase I. At 298 K and 1 bar, the (010) surface showed an absolute adsorption capacity of 0.214 mmol/g. At the same conditions, an interaction energy of - 10.1 kJ/mol was observed, the highest obtained throughout all simulations. Furthermore, a high adsorption capacity of 10.87 mmol/g was obtained at 45 bar; coupled with this high adsorption capacity, however, was a very weak interaction energy of - 4 kJ/mol. This same trend was observed in the results of phase I.

5.2.3 Comparison to Existing Adsorbents

To fully appreciate the results obtained in sections 5.2.1 and 5.2.2, a direct comparison to existing adsorbents is needed. To accompany our results, and for the sake of clarity, literature comparisons will only examine adsorption capacities at 298 K and 1 bar. Carbon based adsorbents (see section 2.3.3) have previously shown adsorption capacities substantially higher than the values obtained for crystalline urea. At ambient conditions, non-functionalised microporous aerogels have shown CO_2 adsorption capacities > 3.0 mmol/g, whilst activated carbons have shown capacities > 5.6 mmol/g at the same conditions.[79,80] Furthermore, in 2013 Alhwaige *et al* published a bio-based chitosan hybrid aerogel with a capacity of 4.15 mmol/g; this material also showed good stability in cyclic adsorption-desorption processes.[81] The literature also shows that Molecular Organic Frameworks show CO_2 adsorption capacities ranging from 1.0 - 4.0 mmol/g at ambient conditions.[82] It is clear from a brief survey of the literature, that at ambient conditions, many commonly studied adsorbents show much greater capacities than crystalline urea. Despite this, there are many other properties to consider when developing new adsorbents. In this work, the only properties assessed were the adsorption capacities and interaction strengths. Therefore, at this moment in time, if these are the only properties to be taken into account, it is of the authors opinion that the use of crystalline urea as a carbon capture adsorbent should be avoided.

5.2.4 Temperature Effects in CO_2 Adsorption

To study how temperature affects the adsorption properties of urea, the surface with the highest adsorption capacity (001) was simulated at a range of different temperatures. At around 4 million steps, all simulations had reached an

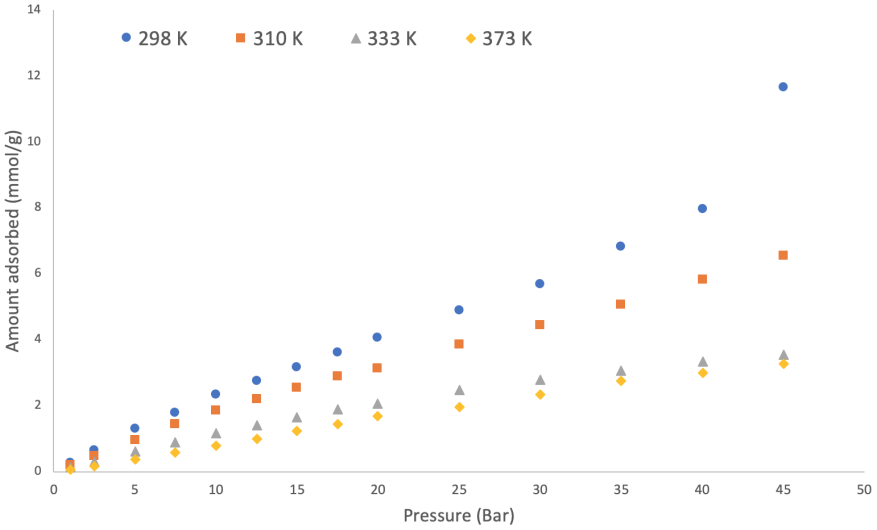

Figure 15: Excess uptake of CO_2 at 298 K, 310 K, 333 K and 373 K on the (001) surface of ambient-phase urea.

equilibrium amount of CO_2 molecules, thus indicating that the chosen number of steps (10 million) was sufficient to obtain reliable statistics.

Figure 15 shows the effect that increasing temperature has on the adsorption capacity. It is evident that an increase in temperature drastically reduces the adsorption characteristics of urea. At 298 K and ambient pressure, the excess uptake shown by (001) was 0.250 mmol/g. At 373 K, a much reduced capacity of 0.061 mmol/g was observed.

The results further show that the gradient of the adsorption isotherms increases as the temperature is decreased. This leads to increased adsorption at the same pressures with lower temperatures. This phenomenon should be relatively easy to explain - at higher temperatures, CO_2 molecules have increased kinetic energy, thus increasing movement and allowing them to overcome the attractive interactions between themselves and the crystal framework. It is apparent from the results that a relatively narrow spectrum of pressures were assessed; it is common in the literature for studies to assess isotherms at a wider range of pressures.[54] However, in this study, the narrow spectrum was chosen for two reasons: (i) to mimic the 'typical' pressures used in industrial carbon capture processes and (ii) to probe the most common range of pressures examined in the literature for novel carbon capture adsorbents.

5.2.5 Mixed Component Isotherms: CO_2/N_2 Selectivity

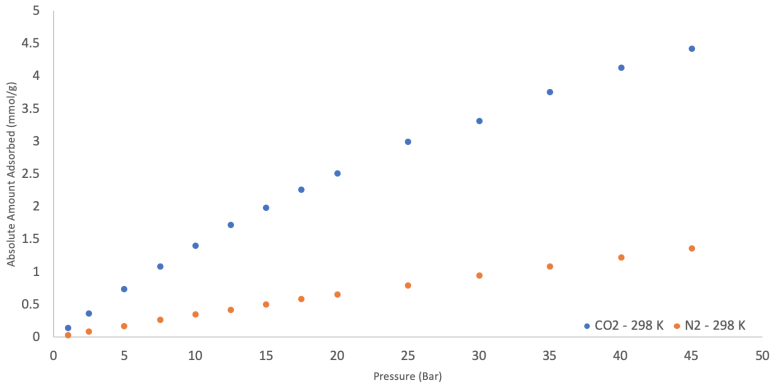

Figure 16: Mixed-component adsorption isotherms for carbon dioxide and nitrogen gas on the (001) surface of phase I urea.

The composition of flue gas can vary greatly. In a natural gas-fired power plant, flue gas composition is typically as follows: 8-10 % CO_2, 18 - 20 % H_2O and 67 - 72 % N_2.[83] For this reason, the selectivity of urea towards CO_2 in the presence of N_2 gas was assessed. To examine urea selectivity, the phase I surfaces were used for multi-component GCMC simulations. Figure 16 shows the mixed component adsorption isotherm for (001) between the pressures of 1 - 45 bar. Is is evident from Figure 16 that urea shows some degree of selectivity towards CO_2. At 1 bar pressure, the amount adsorbed of CO_2 was 0.14 mmol/g. At the same pressure, 0.035 mmol/g of N_2 was adsorbed, meaning that a CO_2 selectivity of ≈ 4 was observed.

Furthermore, Figure 17 shows the adsorption of CO_2 and N_2 on the (100) surface. Unsurprisingly, as seen in section 5.2.1, the adsorption of CO_2 (in the presence of N_2) on (100) was notably less than the (001) surface. At 1 bar, the (100) surface showed a CO_2 adsorption capacity of 0.05 mmol/g, compared to a value of 0.14 mmol/g observed on the (001) surface.

At 40 bar, the (100) and (001) surfaces showed CO_2 adsorption capacities of 2.02 and 4.12 mmol/g respectively. The overall trend, however, is as follows: at lower pressures, and in the presence of nitrogen, the (001) surface shows ≈ 3 times greater adsorption than the (100) surface. Yet once higher pressures are reached, this value reduces and approximately twice as much adsorption is demonstrated by the (001) surface.

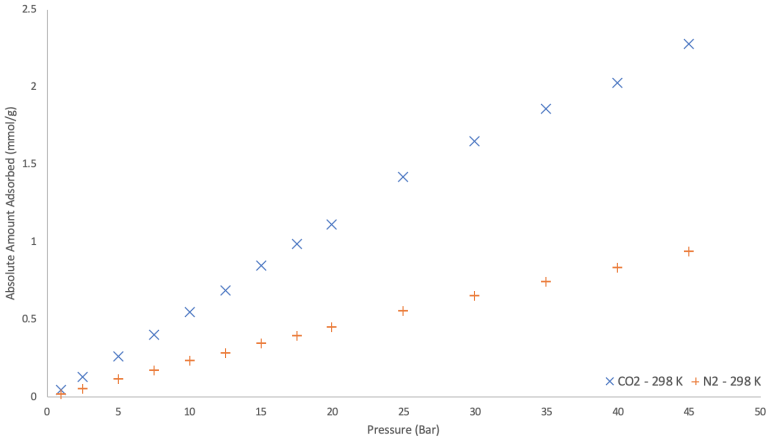

Figure 17: Mixed-component adsorption isotherms for carbon dioxide and nitrogen gas on the (100) surface of phase I urea.

At each pressure point, the amount of CO_2 adsorbed was divided by the amount of N_2 adsorbed; this calculates a value for the selectivity of urea towards CO_2. Figure 18 shows the selectivity of the two surfaces of phase I towards CO_2. The results in Figure 18 are very interesting to observe. The first clear result is that (001) shows twice the selectivity compared to the (100) surface. Also, between pressures of 1 - 50 bar, the trend in selectivity is very interesting; (100) shows greater selectivity at higher pressures, whilst (001) shows greater selectivity at lower pressures. Industrial processes for carbon capture typically want to operate at lower pressures with high selectivity. Therefore, one key conclusion can be drawn from these results: for an efficient adsorption process using urea, (001) is the most desirable surface to have exposed at the crystal-air interface.

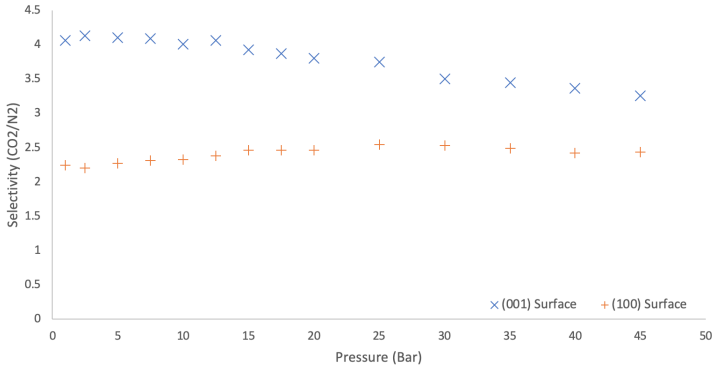

Figure 18: Selectivity of (100) and (001) towards carbon dioxide gas in the presence of nitrogen gas.

Chapter 6

Conclusions and Further Work

To conclude, phase I, phase III and phase IV of urea were computationally investigated as novel adsorbents for use in post-combustion carbon capture. Their crystal structures were obtained from the CCDC, followed by using BFDH theory to predict the predominant surfaces in the three phases of urea. Following this, density functional theory was used to relax the unit cells, and the results showed that ambient phase urea was the most stable crystal structure. Also, the geometry of phase III failed to successfully converge to an energy minima, thus being removed from any future work.

Further to relaxation of the unit cell geometries, slabs of crystalline urea with added vacuum were generated and further relaxed using density functional theory. The chosen surfaces were (100) and (001) from phase I, and (010) from phase IV. Once complete, the relaxed slabs were taken and used to study the adsorption properties of crystalline urea. Monte Carlo methodology was used to simulate adsorption isotherms under conditions imposed by the grand canonical ensemble. The results showed that the (001) surface in ambient phase urea had the highest adsorption of all chosen surfaces. Furthermore, mixed component isotherms showed that the (100) surface in phase I urea demonstrates a selectivity of ≈ 2 towards CO_2 (in the presence of N_2), whilst the (001) surface shows approximately twice this selectivity.

The results of this study showed that the **direct** use of crystalline urea as an

adsorbent for carbon capture is not recommended. However, more work should be carried out to further assess the adsorption properties of urea. Further simulations should be performed to assess the adsorption of CO_2 in confined 'cavities' of urea; this could be achieved by simulating two surfaces at chosen, fixed separating distances within the same simulation cell. Furthermore, if urea were to be utilised as an adsorbent, it would likely be combined into a bio-based framework that alters its adsorption properties. The authors propose the embedding of urea into a micro-porous polymeric cellulosic membrane; this could directly alter the adsorption properties of the material, and should therefore be investigated. To fully assess the framework properties of cellulose, simulations could be performed where urea is encapsulated into a cellulosic matrix. This could give insight into how a polymeric membrane may affect the adsorption capacity and selectivity of urea towards CO_2.

Bibliography

[1] S. Moser and L. Dilling, *Environment*, 2004, **46**, 32–46.

[2] M. Rahman, *Interdisciplinary Description of Complex Systems*, 2013, **11**, 1–13.

[3] J. Hansen, I. Fung, A. Lacis, D. Rind, G. Russel, S. Lebendeff, R. Ruedy and P. Stone, *Journal of Geophysical Research*, 1988, **93(D8)**, 9314–9364.

[4] C. J. Vörösmarty, P. Green, J. Salisbury and R. B. Lammers, *Science*, 2000, **289**, 284–288.

[5] Cynthia Rosenzweig and Martin L. Parry, *Nature*, 1994, **367**, 133 – 138.

[6] C. D. Butler, *International Journal of Environmental Research and Public Health*, 2018, **15**, 1–21.

[7] United Nations Framework and Convention on Climate Change, *Paris Agreement*, United nations technical report, 2015.

[8] G. Althor, J. E. M. Watson and R. A. Fuller, *Nature Publishing Group*, 2016, **6**, 1–6.

[9] R. J. Scholes, D. W. R. Wallace, D. Archer, M. R. Ashmore, O. Aumont, D. Baker, M. Battle, M. Bender, L. P. Bopp, P. Bousquet, K. Caldeira, P. Ciais, P. M. Cox, W. Cramer, F. Dentener, I. G. Enting, C. B. Field, P. Friedlingstein, E. A. Holland, R. A. Houghton, J. I. House, A. Ishida, A. K. Jain, I. A. Janssens, F. Joos, T. Kaminski, C. D. Keeling, R. F. Keeling, D. W. Kicklighter, K. E. Kohfeld, W. Knorr, R. Law, T. Lenton, K. Lindsay, A. C. Manning, R. J. Matear, A. D. Mcguire, J. M. Melillo,

R. Meyer, M. Mund, J. C. Orr, S. Piper, K. Plattner, P. J. Rayner, S. Sitch, R. Slater, S. Taguchi, P. P. Tans, H. Q. Tian, M. F. Weirig, T. Whorf and A. Yool, *The Carbon Cycle and Atmospheric Carbon Dioxide*, Ipcc technical report, 2013.

[10] S. Solomon, D. Qin and M. Manning, *AR4 Climate Change 2007: Summary for Policymakers*, Ipcc technical report, 2007.

[11] M. North and P. Styring, *Faraday Discussions*, 2015, **183**, 489–502.

[12] D. Y. C. Leung, G. Caramanna and M. M. Maroto-valer, *Renewable and Sustainable Energy Reviews*, 2014, **39**, 426–443.

[13] A. A. Olajire, *Energy*, 2010, **35**, 2610–2628.

[14] Global CCS Institute, *The Global Status of CCS*, Global carbon capture and storage institute technical report, 2018.

[15] T. Wilberforce, A. Baroutaji, B. Soudan, A. H. Al-alami and A. Ghani, *Science of the Total Environment*, 2019, **657**, 56–72.

[16] IUPAC, *Compendium of Chemical Terminology*, Blackwell Science, Zurich, 1997, p. 85.

[17] G. Corp, *"Seperating Acid Gases"*, 1930.

[18] M. Bui, C. S. Adjiman, A. Bardow, E. J. Anthony, A. Boston, S. Brown, P. S. Fennell, S. Fuss, A. Galindo, L. A. Hackett, J. P. Hallett, H. J. Herzog, G. Jackson, J. Kemper, S. Krevor, G. C. Maitland, M. Matuszewski, I. S. Metcalfe, C. Petit, G. Puxty, J. Reimer, D. M. Reiner, E. S. Rubin, S. A. Scott, N. Shah, B. Smit, J. P. Trusler, P. Webley, J. Wilcox and N. Mac Dowell, *Energy and Environmental Science*, 2018, **11**, 1062–1176.

[19] G. T. Rochelle, *Absorption-Based Post-combustion Capture of Carbon Dioxide*, Woodhead Publishing, 2016, pp. 35–66.

[20] G. Rochelle, E. Chen, S. Freeman, D. Van Wagener, Q. Xu and A. Voice, *Chemical Engineering Journal*, 2011, **171**, 725–733.

[21] L. V. Van Der Ham, M. C. Romano, H. M. Kvamsdal, D. Bonalumi, P. Van Os and E. L. Goetheer, *Energy Procedia*, 2014, **63**, 1218–1222.

[22] E. Oko, M. Wang and A. S. Joel, *International Journal of Coal Science and Technology*, 2017, **4**, 5–14.

[23] S. B. Fredriksen and K. J. Jens, *Energy Procedia*, 2013, **37**, 1770–1777.

[24] N. Hajilary, A. Ehsani Nejad, S. Sheikhaei and H. Foroughipour, *Journal of Petroleum Science and Technology*, 2011, **1**, 24–30.

[25] A. H. Berger and A. S. Bhown, *Energy Procedia*, 2011, **4**, 562–567.

[26] R. Ben-Mansour, M. A. Habib, O. E. Bamidele, M. Basha, N. A. Qasem, A. Peedikakkal, T. Laoui and M. Ali, *Applied Energy*, 2016, **161**, 225–255.

[27] G. P. Hammond and J. Spargo, *Energy Conversion and Management*, 2014, **86**, 476–489.

[28] M. T. Ho, G. W. Allinson and D. E. Wiley, *Industrial and Engineering Chemistry Research*, 2008, **47**, 4883–4890.

[29] C. Voss, *Adsorption*, 2005, **11**, 527–529.

[30] C.-t. Chou, F.-h. Chen, Y.-j. Huang and H.-s. Yang, *Chemical Engineering Transactions*, 2013, **32**, 1855–1860.

[31] D. Marx, L. Joss, M. Hefti and M. Mazzotti, *Industrial and Engineering Chemistry Research*, 2016, **55**, 1401–1412.

[32] M. Clausse, J. Bonjour and F. Meunier, *Chemical Engineering Science*, 2004, **59**, 3657–3670.

[33] C. A. Grande, *ISRN Chemical Engineering*, 2012, **2012**, 1–13.

[34] M. Moshoeshoe, M. S. Nadiye-Tabbiruka and V. Obuseng, *American journal of Materials Science*, 2017, **7**, 191–221.

[35] N. Mehio, S. Dai and D. E. Jiang, *Journal of Physical Chemistry A*, 2014, **118**, 1150–1154.

[36] Y. Li, H. Yi, X. Tang, F. Li and Q. Yuan, *Chemical Engineering Journal*, 2013, **229**, 50–56.

[37] H. C. Zhou, J. R. Long and O. M. Yaghi, *Chemical Reviews*, 2012, **112**, 673–674.

[38] M. Ding, R. W. Flaig, H. L. Jiang and O. M. Yaghi, *Chemical Society Reviews*, 2019, **48**, 2783–2828.

[39] C. A. Trickett, A. Helal, B. A. Al-maythalony, Z. H. Yamani, K. E. Cordova and O. M. Yaghi, *Nature Publishing Group*, 2017, **2**, 1–16.

[40] Z. Zhang, Y. Zhao, Q. Gong, Z. Li and J. Li, *Chemical Communications*, 2013, **49**, 653–661.

[41] A. E. Creamer and B. Gao, *Environmental Science and Technology*, 2016, **50**, 7276–7289.

[42] Z. Chen, S. Deng, H. Wei, B. Wang, J. Huang and G. Yu, *Frontiers of Environmental Science and Engineering*, 2013, **7**, 326–340.

[43] E. E. Ünveren, B. Ö. Monkul, e. Sarıoğlan, N. Karademir and E. Alper, *Petroleum*, 2017, **3**, 37–50.

[44] E. Urban, *Journal of Applied Electrochemistry*, 2016, **46**, 1011–1029.

[45] M. K. Corpinot and D. K. Bučar, *Crystal Growth and Design*, 2019, **19**, 1426–1453.

[46] M. Younas, M. Sohail, L. L. Kong, M. J. Bashir and S. Sethupathi, *International Journal of Environmental Science and Technology*, 2016, **13**, 1839–1860.

[47] Yara, *Yara Fertilizer Industry Handbook*, Yara technical report, 2018.

[48] D. Dollimore, P. Spooner and A. Turner, *Surface Technology*, 1976, **4**, 121–160.

[49] R. L. Harrison and M. Carlo, *Introduction to Monte Carlo Simulation*, National institute of health technical report, 2011.

[50] D. Dubbeldam, A. Torres-Knoop and K. S. Walton, *Molecular Simulation*, 2013, **39**, 1253–1292.

[51] Y. Liu and J. Wilcox, *International Journal of Coal Geology*, 2012, **104**, 83–95.

[52] J. Jiang and S. I. Sandler, *Journal of American Chemical Society*, 2005, **127**, 11989–11997.

[53] A. Fraccarollo, L. Canti, L. Marchese, M. Cossi and T. Michel, *Langmuir*, 2014, **30**, 4147–4156.

[54] Y. Kurniawan, S. K. Bhatia and V. Rudolph, *AIChE*, 2006, **52**, 957–967.

[55] K. Roszak and A. Katrusiak, *Journal of Physical Chemistry C*, 2017, **121**, 778–784.

[56] N. Sklar, M. E. Senko and B. Post, *Acta Crystallographica*, 1961, **14**, 716–720.

[57] Cambridge Crystallographic Data Centre, *Mercury*, 2019, `https://www.ccdc.cam.ac.uk/solutions/csd-system/components/mercury/`.

[58] R. Docherty, G. Clydesdale, J. Roberts and P. Bennema, *Journal of Physics D: Applied Physics*, 1991, **24**, 89–99.

[59] S. Elhadj, J. J. De Yoreo, J. R. Hoyer and P. M. Dove, *Proceedings of the National Academy of Sciences*, 2006, **103**, 19237–19242.

[60] F. Jensen, *Introduction to Computational Chemistry*, John Wiley & Sons Ltd, Sussex, 2007, vol. 90, p. 232.

[61] P. Hohenberg and W. Kohn, *Phys. Rev.*, 1964, **136**, B864–B871.

[62] E. DobardŽić, M. Dimitrijević and M. V. Milovanović, *Physical Review B - Condensed Matter and Materials Physics*, 2015, **91**, 1–11.

[63] H. S. Yu, S. L. Li and D. G. Truhlar, *Journal of Chemical Physics*, 2016, **145**, 2–3.

[64] J. VandeVondele and O. Schutt, *CP2k*, 2019.

[65] T. Rohwedder and R. Schneider, *Journal of Mathematical Chemistry*, 2011, **49**, 1889–1914.

[66] T. H. Fischer and J. Almlöf, *Journal of Physical Chemistry*, 1992, **96**, 9768–9774.

[67] G. X. Zhang, A. M. Reilly, A. Tkatchenko and M. Scheffler, *New Journal of Physics*, 2018, **20**, 0–19.

[68] S. Izzaouihda, H. Abou El Makarim, D. M. Benoit and N. Komiha, *Journal of Physical Chemistry C*, 2017, **121**, 20259–20265.

[69] J. VandeVondele and J. Hutter, *Journal of Chemical Physics*, 2007, **127**, 1–10.

[70] D. Frenkel, *Introduction to Monte Carlo Methods*, 2004, vol. 23, pp. 29–60.

[71] N. Metropolis, A. W. Rosenbluth, M. N. Rosenbluth, A. H. Teller and E. Teller, *The Journal of Chemical Physics*, 1953, **21**, 1087–1092.

[72] J. J. Potoff and J. I. Siepmann, *AIChE Journal*, 2001, **47**, 1676–1682.

[73] F. Siperstein, A. L. Myers and O. Talu, *Molecular Physics*, 2002, **100**, 2025–2030.

[74] E. Gdoutos, R. Agrawal and D. Espinosa, *Proceedings of the 2011 American Control Conference*, 2010, **84**, 1541–1551.

[75] S. Brandani, E. Mangano and L. Sarkisov, *Adsorption*, 2016, **22**, 1–16.

[76] A. L. Myers and P. A. Monson, *Langmuir*, 2002, **18**, 10261–10273.

[77] R. Tran, Z. Xu, B. Radhakrishnan, D. Winston, W. Sun, K. Persson and S. Ping Ong, *Nature Scientific Data*, 2016, **80**, 1 – 13.

[78] C. G. Jacobsen, *Nature Materials*, 2005, **4**, 186.

[79] C. Robertson and R. Mokaya, *Microporous and Mesoporous Materials*, 2013, **179**, 151–156.

[80] S. Y. Lee and S. J. Park, *Journal of Colloid and Interface Science*, 2013, **389**, 230–235.

[81] A. A. Alhwaige, T. Agag, H. Ishida and S. Qutubuddin, *RSC Advances*, 2013, **3**, 16011–16020.

[82] J. Wang, L. Huang, R. Yang, Z. Zhang, J. Wu, Y. Gao, Q. Wang, D. O'Hare and Z. Zhong, *Energy and Environmental Science*, 2014, **7**, 3478–3518.

[83] C. Song, W. Pan, S. T. Srimat, J. Zheng, Y. Li, Y. H. Wang, B. Q. Xu and Q. M. Zhu, *Studies in Surface Science and Catalysis*, 2004, **153**, 315–322.